universität wien

MASTERARBEIT

Titel der Masterarbeit

„Detection of Cervical Cancer Derived Circulating Tumor Cells in the Peripheral Blood“

verfasst von

Markus Arnold Niebuhr BSc

angestrebter akademischer Grad

Master of Science (MSc)

Wien, Mai 2015

Studienkennzahl lt. Studienblatt:	A 066 830
Studienrichtung lt. Studienblatt:	Molekulare Mikrobiologie, Mikrobielle Ökologie und Immunbiologie
Betreut von:	Ao.Univ.-Prof. Dr. Robert Zeillinger

Tables of Contents

1 Introduction

1.1 Overview

Cervical cancer is the fourth most common cancer in women worldwide with an estimated 528,000 new cases and 266,000 deaths per year [1]. With an occurrence rate of around 70%, cervical cancer cases mostly emerge in developing countries, where public health infrastructure does not provide routine cytological screening [1, 2]. The main cause of cervical cancer is by far the Human papilloma virus (HPV). Until today more than 150 HPV genotypes are known, of which at least 12 are carcinogenic [3, 4]. During carcinogenic cellular proliferation of malignant tumors, detachment and invasion of tumor cells into blood or lymphatic vessels is a common route for dissemination. These circulating tumor cells are transported to distant organs by the blood stream, where extravasation and establishment of a tumor microenvironment might lead to metastasis [5].

Detection and characterization of circulating tumor cells could lead to a better understanding of the disease and might be a tool for disease monitoring and relapse diagnosis of cervical cancer. Therefore, the main goal of this study is the identification of an antigen based marker panel, which allows a specific blood-based detection of cervical cancer derived circulating tumor cells. This panel should on the one hand include markers specific for cell cycle progression and epithelial cells, on the other hand antibodies able to detect human papillomavirus proteins.

1.2 Cervical cancer

Cervical cancer is a neoplasia of the cervix uteri. It develops between the columnar epithelium and the squamous epithelium of the ectocervix. Both epithelia are highly metaplastic during lifetime with peaking activity during puberty and after the first pregnancy [1]. Nearly all cervical cancer cases (99.7%) are directly linked to an infection with high-risk HPV genotypes [6]. With an overall HPV prevalence rate of 10.4% in 2007, about 291 million women carried the virus in the cervix at all times [7]. Although, other risk factors as for example smoking or long term intake of contraceptives have been reported, they seem to be of minor importance [8]. In a global view, the incidence of cervical cancer cases is highest in developing countries with more than 70% new cases in 2012 (figure 1). Additionally, the mortality rate in this countries is above 85% [1]. In contrast the incidence and mortality rate in Europe and North America allocates less than 15% of the global numbers. This comparatively low cervical cancer rate is due to cervical dysplasia routine examination and established genotype specific HPV vaccination [9].

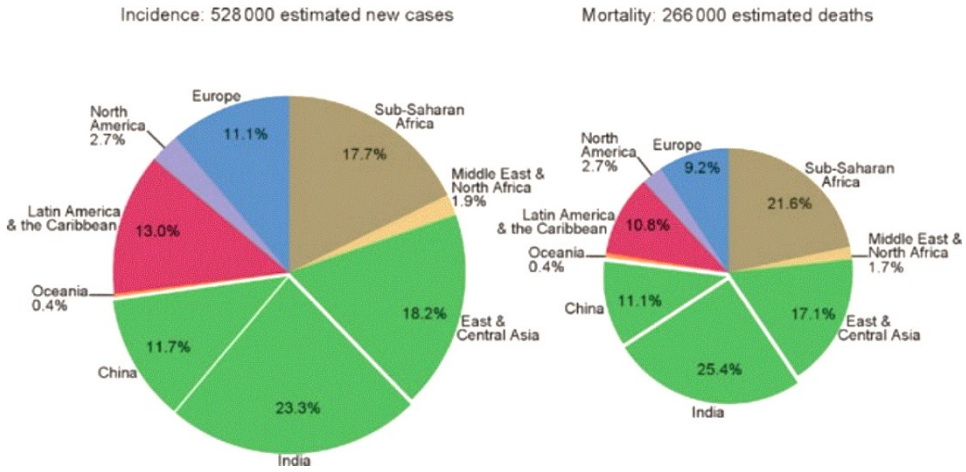

Figure 1: Global estimation of new cervical cancer cases and mortality in 2012. The majority of new cervical cancer cases and the consequential death is mainly located in developing countries (Illustration adapted from [1])

1.2.1 Progression and staging

The formation of cervical cancer is characterized by a benign preliminary phase of cervical intraepithelial neoplasia (CIN) (figure 2). This precancerous CIN phase, with characteristic abnormal morphological changes, is divided into definite histological grades ranging from CIN 1 to CIN 3 [10]. The CIN classification is mainly based on the occupation rate of abnormal cells during metaplasia and is clinically accomplished by Pap-cytology [11]. CIN grade 1 represents a mild dysplasia of the lower third cervical epithelium, often associated with low-risk HPV infections. In addition altered cells often undergo koilocytosis, which is associated with nuclear enlargement and deviating nuclear membrane structure [12]. Aberrations of this grade are often cleared by the immune system, although an entire clearance might take for years. CIN grade 2 is a moderate dysplasia with up to two-thirds of the cervical epithelium occupied by neoplastic cells. In CIN grade 3 more than two-thirds or the entire cervical epithelium are made up by aberrant neoplastic cells. Both CIN 2 and CIN 3 are usually caused by high-risk HVP genotypes and are associated with viral DNA integration [13]. Moreover, the majority will persist without considerable immunological clearance with a small fraction developing invasive carcinoma [14].

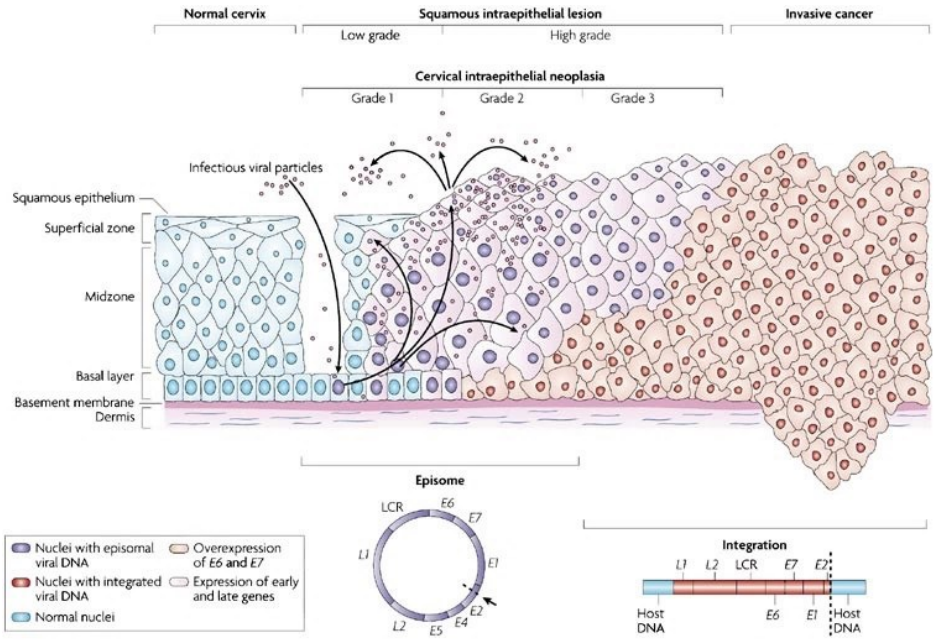

Figure 2: Cellular dysplasia in cervical cancer progression HPV mediated dysplasia in cervical cancer progression. CIN 1: Basal cells are infected by HPV, episomal replication of viral genome and little virion release. CIN 2: Beginning integration of viral DNA in host genome, starting overexpression of E6/E7 in the basal layer and broader virion release. CIN 3: Plain proliferation of aberrant cells with integrated viral genome and predominantly E6/E7 overexpression in spinous epithelia. Cervical cancer: Plainest proliferation of E6/E7 overexpressing cells in the entire epithelia, further invasive cancerous growth with subdermal invasion. (Illustration adapted from [13])

Formation of invasive cervical carcinoma is a prolonged process often requiring 10 to 20 years of CIN persistence. It is characterized by prevalent viral DNA integration, occupation of the whole cervical epithelium by dysplastic cells and mainly the budding of cancerous cells into the stroma (figure 2) [10]. From the hallmark of epithelial barrier disruption onwards, tumor cells may spread in the surrounding stroma.

The clinical classification of cervical cancer is defined by the International Federation of Obstetricians and Gynaecologists (FIGO) and mainly comprises the carcinoma size and invasive spread (table 1).

Table 1: FIGO stages of cervical cancer. [15]

FIGO stage	Pathologic Characteristics
0	**Cervical intraepithelial neoplasia (CIN III)**
I	**Carcinoma confined to the cervix**
IA	Invasive carcinoma only diagnosed by microscopy
IA1	Measured stromal invasion ≤ 3.0 mm in depth and ≤ 7.0 mm in horizontal spread
IA2	Measured stromal invasion > 3.0 mm and ≤ 5.0 mm with a horizontal spread ≤ 7.0 mm
IB	Carcinoma confined to the cervix or microscopic lesion greater than IA2
IB1	Clinically visible lesion <4 cm in greatest dimension
IB2	Clinically visible lesion >4 cm in greatest dimension

II		**Carcinoma invades beyond the cervix but not to pelvic wall or to lower third of vagina**
	IIA	Upper two-thirds of vagina are affected without parametrial invasion
	IIA1	Clinically visible lesion <4 cm in greatest dimension
	IIA2	Clinically visible lesion >4 cm in greatest dimension
	IIB	Upper two-thirds of vagina are affected with parametrial invasion
III		**Carcinoma extends to pelvic wall and/or involves lower third of vagina and/or causes hydronephrosis or nonfunctional kidney**
	IIIA	Carcinoma involves the lower third of the vagina with no extension to pelvic sidewall
	IIIB	Extension to the pelvic wall and/or hydronephrosis or non-functioning kidney
IV		**The carcinoma has extended beyond the true pelvis or has involved (biopsy proven) the mucosa of the bladder or rectum**
	IVA	Spread of the growth to adjacent organs
	IVB	Spread to distant organs

In addition to the FIGO staging, the pathological inspection assesses the degree of differentiation by applying a grading scheme. Low grade (G1) for well-differentiated tumor cells, intermediate grade (G2) for moderately differentiated tumor cells and high grade (G3) for poorly differentiated tumor cells.

1.2.2 Clinical course

In a large number of cases, patients with CIN and early cervical cancer stages are free of complaints. In advanced stages abnormal bleeding and abdominal pain may occur. Thus, the routine cervical dysplasia screening for early detection is of major importance. Clinical diagnostic methods mainly rely on Pap-cytology, colposcopy, HPV testing and serum tumor markers. However, the specificity and sensitivity of the primarily used serum tumor markers Cancer-Antigen 125 (CA125) and Carcinoembryonic antigen (CAE) is in most cases insufficient for a precise diagnosis, especially since either marker might be up regulated in benign or inflammatory diseases [16]. The general treatment of cervical cancer is patient-specific, but primarily comprises chemotherapy, radiation therapy and surgery. Following the primary treatment, the relapse monitoring contains similar screening techniques with additional integration of routine X-ray studies [16]. Therapeutic success and clinical remission are also case-dependent and complex. In general, higher age, higher FIGO stage, lymph node metastases and radiotherapy or chemotherapy are worsening prognosis [17]. In addition, the formation of distant metastases affects the overall therapeutic success. These metastases are difficult to detect and treat with the currently available screening methods, once they spread outside the pelvis [18]. Out of successful established micrometastases a reappearing tumor growth may occur, causing clinical relapse. Early indications for recurrence are difficult to detect and the general performance of, especially, serum tumor markers is controversial [16].

1.3 Human papillomavirus

The human papilloma virus is a double-stranded DNA virus from the taxonomic family of Papillomaviridae. The viral genome is organized circularly with a size of approximately 8 kb. It encodes for 9 genes, 7 so called early genes, encoding for proteins involved in replication and integration and 2 late genes, responsible for capsid structure proteins (figure 3).

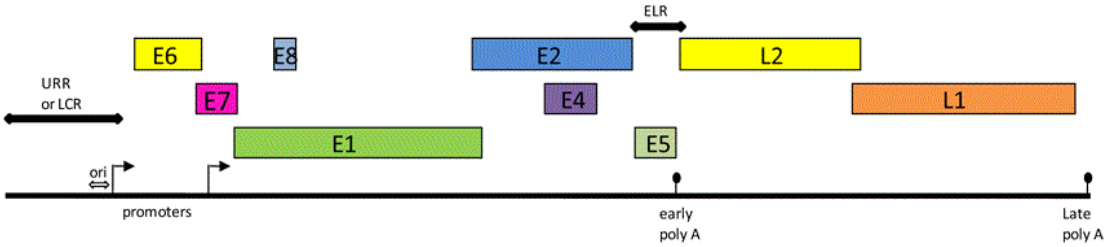

Figure 3: HPV genome organization in linear consideration. Early genes encode for proteins associated with replication, genome integration and aberrant cell cycle establishment. Late gene products are viral capsid-structure proteins. (Illustration obtained from: http://pave.niaid.nih.gov/#explore/proteins/protein_information, 27.03.2015)

Over the last years the genomic data of more than 150 human subtypes and 60 animal papillomaviruses have been published and facilitated a taxonomical classification [4]. Representatives of every genus (Alpha, Beta, Gamma and mu types) are known to cause warts and genital lesions, but typically no neoplasia [19]. These mild progressing viruses are classified as ‘low-risk’ genotypes. In contrast to these benign genotypes, the WHO (World Health Organization) classifies 12 HPV strains (HPV 16, 18, 31, 33, 35, 39, 45, 51, 52, 56, 58 and 59) as malign ‘high-risk’ and probably cancer-causing viruses [4, 20]. All high-risk strains are Alpha papillomaviruses, emerging from a defined phylogenetic branch, which seems to be genetically prone to malignancy [20]. From all of the high-risk strains with clinical relevance, HPV 16 (57%) and 18 (16%) exhibit the highest incidence rate [1]. Furthermore, HPV is the most sexually transmitted infection worldwide. During lifetime, 75% of all sexually active woman are exposed to HPV [6]. The group of young women, aged 20 - 35 years, shows the highest prevalence of HPV infections with a high-risk HPV infection rate of up to 30% [21]. Low-risk HPV infections of the cervix are rarely detectable and often diminish within 12 to 18 month. On the contrary, high-risk strains carry the ability to persist for years without immune mediated clearance [20, 22]. This enduring infection is mainly arbitrated by the genetic constitution and cellular levels of the HPV proteins E6 and E7 [23]. These viral proteins are the key-contributors towards cell aberration and carry pleiotropic capabilities pushing the infected cell towards malignancy.

1.3.1 Lifecycle

The lifecycle of HPV is highly specific compared to other virus families. For successful infection and proliferation, HPV depends on epidermal or mucosal epithelial cells of the basal layer (figure 4) [24]. The range of possible infection sites extends from the entire

skin to reproduction organs. In most viruses the viral reproduction is initiated upon infection. However, viral replication in HPV infected cells does not start immediately post-infection. The virus only replicates after the host cell has undergone mitosis and infected daughter cells start to differentiate [25].

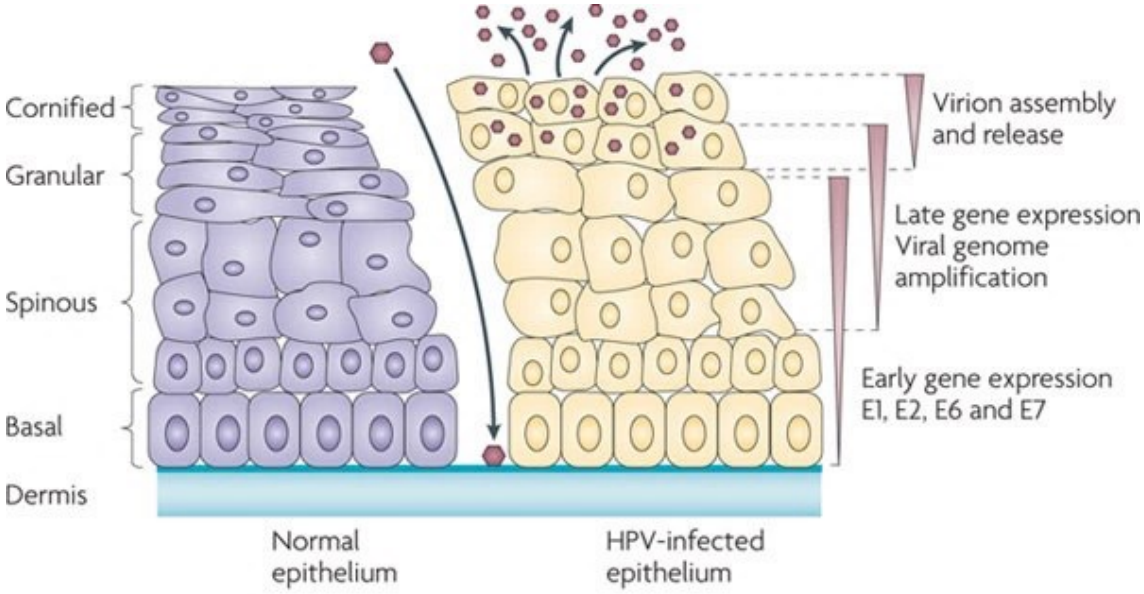

Figure 4: Lifecycle of the human papillomavirus. Virion infection of the basal cell layer. Gene expression and genome integration into host chromosome in lower epidermal layer. Virus assembly and release in outer epidermal layer. (Illustration adapted from [25])

After infection the first detectable expression of viral genes is conspicuously delayed and occurs 12 - 24 hours after virus mediated surface binding [26]. Following the infection, the viral genome is established extrachromosomal in the form of episomes [25]. Since HPV does not encode for a DNA polymerase nor other enzymes involved in protein biosynthesis, the viral gene expression entirely relies on the host machinery. In early infection phase the expression of E1 and E2 was shown to be crucial [20]. There is evidence, which features E1 and E2 as initiators of replication-decoupling from the host cell [27]. L2 was found to play an important role for integration in the host genome. Therefore, L2 interacts with the motor protein Dynein and facilitates the chromosomal dislocation via the microtubule network towards the nucleus [28]. Although the precise translocation mechanism is not fully understood, the consistent position favors the exploit of nuclear envelope breakdown during mitosis, rather than active transport into the nucleus for integration [29]. The actual genome integration of HPV is most likely mediated by non-homologous sequence-specific recombination due to several consensus sequences among the viral and human genome integration sites [30]. Coincident to genome integration, expression of E6 and E7 is initiated. Both gene products are strong proliferation drivers and play a considerable role in the HPV altered dermal differentiation.

Following the initial infection, viral replication and late gene expression is progressing in the spinous layer. During amplification a cellular viral load of approximately 50 – 100 viral copies per cell is established and maintained [31]. In the ongoing epidermal matu-

ration and outward differentiation viral assembly is accomplished. Ultimately, in the granular and cornified layer, mature virions are released in the surrounding tissue capable of infection.

1.3.2 HPV oncoproteins

The proteins E5, E6 and E7 are the main contributors of HPV associated malignant conversion. The pleiotropic functionality ranges from cell cycle aberration, transmembrane signaling, immortalization to chromosomal instability [6]. Molecular pathways involving HPV oncoproteins are depicted in figure 5.

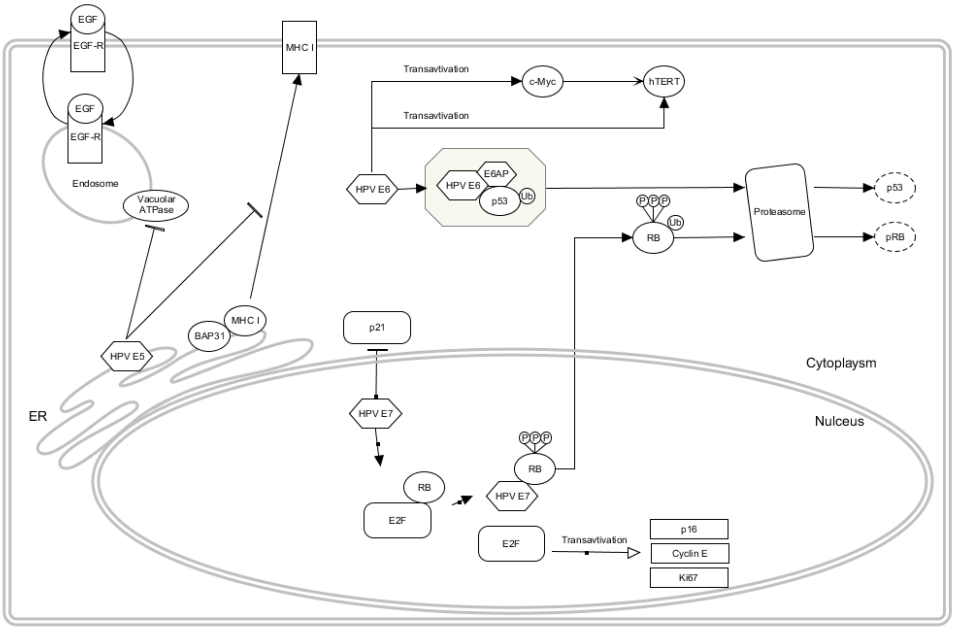

Figure 5: Cellular function of the HPV oncoproteins E5, E6 and E7. E5 plays an important role in cell-growth induction. E6 and E7 are involved in S-phase induction, inhibition of apoptosis and lead to immortalization.

1.3.2.1 HPV E5

The HPV E5 protein is a hydrophobic transmembrane protein, which is expressed in the early to late region of the viral genome (figure 3). E5 is not constitutively expressed among all known HPV strains and ranges in size from approximately 40 to 85 amino acids [32]. It is primarily localized in the endoplasmic reticulum [33]. Despite its later expression, HPV E5 seems to play an important role in the early stages of malignant development. For early enhanced cell proliferation, membrane-bound E5 affects the epidermal growth factor (EGF) recycling by preventing endosomal acidification and subsequently inhibition of proteasomal degradation [33]. Thus, the membrane level of the EGF receptor is elevated in HPV E5 expressing cells, enhancing the external growth stimulus by EGF. Furthermore, HPV E5 contributes towards immune evasion by inhibiting the MHC class I membrane-exposition. In fact E5 impairs synthesis, stability and transport towards the membrane by maintaining its localization in the Golgi appa-

ratus [34]. Although the cellular expression and MHC class I assembly remains unaffected. With cancerous progression the cellular effect and importance of HPV E5 diminishes and subsequently disappears [24]. This is caused by a loss of a major E5 coding sequence during genome integration [35]. Hence, HPV E5 plays a substantial role in the development and establishment of cervical neoplasia, although its contribution in late HPV-mediated cancerogenesis is of minor importance.

1.3.2.2 HPV E6

HPV E6 is an approximately 158 amino acid long protein and consists of two zinc-like fingers-domains, flanked by size-variable N-terminal and C-terminal regions [36]. Due to its chromosomal localization at the HPV-ORI, E6 is expressed in the early stages of infection and plays an important role in the process of malignancy. One of its main oncogenic functions is the promotion of cell proliferation by degrading the tumor suppressor p53. Thus, E6 forms a trimetric complex with p53 and the cellular E3-ligase E6-associated protein (E6-AP) (figure 5). Within this complex, E6 activates the E6-AP-mediated poly-ubiquitination of p53, which subsequently leads to its proteasomal degradation [6]. Furthermore, E6 is able to bind to the DNA-binding motif of p53, preventing its transcriptional stimulation ability [25]. Moreover it has been shown that E6 enables the nuclear dislocation of p53 into the cytoplasm [37]. Until now it remains unclear, whether E6 is masking the nuclear localization signal or selectively elevates the nuclear export [36]. Apart from the direct p53 degradation effect, in long term cervical cancer progression, infected cells accumulate genetically mutations through the absence of p53-mediated DNA repair [25]. Another important step towards malignancy and cellular immortalization is the E6 mediated activation of c-Myc and human telomerase reverse transcriptase (hTERT). An increased telomerase activity in HPV infected cells and the location of c-Myc jointly with the E6-E6-AP complex at the hTERT promotor was shown [38, 39]. Besides p53 elimination, HPV E6 has shown to interfere and alter several other cellular processes such as transcription and DNA replication, epithelial organization, cell-cell adhesion, DNA-repair and immune evasion [6, 36].

1.3.2.3 HPV E7

HPV E7 is an approximately 100 amino acid long viral protein. It consists of the two conserved N-terminal regions CR1 and CR2 and a C-terminal zinc-like finger. Due to the chromosomal localization downstream the ORI and E6, E7 is expressed in early viral infection. The main function of E7 in malignant progression is the binding of pRBs (retinoblastoma protein) pocket domain [40]. Thus, the pRB-E2F complex is segregated. In detail, the CR2 region contains a LXCXE motif, which plays an essential role in binding towards pRBs pocket domain [41]. In the regular cellular progression, histone deacetylases 1 and 2 (HDAC1 and -2) comprise the LXCXE-like motif to interact with pRB [42]. Hence, this interaction leads to detachment of acetyl groups, inhibiting the

gene expression by narrowing the chromatin framework. In HPV infected cells this repressive function of pRB is disabled and the loose chromatin structure further facilitates gene expression. pRB mainly represses genes necessary for G_1-S phase progression and in particular the pRB-E2F complex represses the E2F gene expression by masking required enhancer elements [43]. In HPV infected cells, E7 disrupts the pRB-E2F complex and mediates enhanced pRB phosphorylation and ubiquitination. Thus, cellular pRB is degraded and E2F promotes S-phase progression by activating expression of p16, Cyclin E2 and Ki-67, among others. The second main progression in S-phase, induction mediated by E7, is the inhibition of Cyclin-dependent kinase inhibitor 1A (p21) [44]. The C-terminal residue of E7 was shown to interact with multiple regions of p21 [25, 45]. This interaction leads to a masking of the p21-association domain, whereby the interaction towards downstream proteins is disabled [45]. As a result of pRB degradation and p21 inhibition, the G_1-S-phase checkpoint is abrogated and cell proliferation is maintained. Hence, this constitutive S-phase induction is a crucial step of HPV replication, since HPV relies on the cellular replication machinery [25].

1.3.2.4 Collaboration of E6 and E7 in malignant conversion

Alongside the carcinogenic effects of E6 and E7, solitary expression experiments revealed their dependence in cervical dysplasia and invasive malignancies. The relevance of both oncogenes in carcinogenic transformation was first shown by Münger in 1989. Münger mutated the reading frames of all early genes and determined the subsequent oncogenic and immortalization effects *in vitro*. As main result, Münger found out that E6 and E7 are the only essential proteins for malignant transformation. As validation a knock-down experiment was performed suppressing either individual gene, resulting in obliteration of carcinogenic transformation [46]. However, E6 and E7, taken individually, induce cellular aberrations involved in the process of transformation (figure 6).

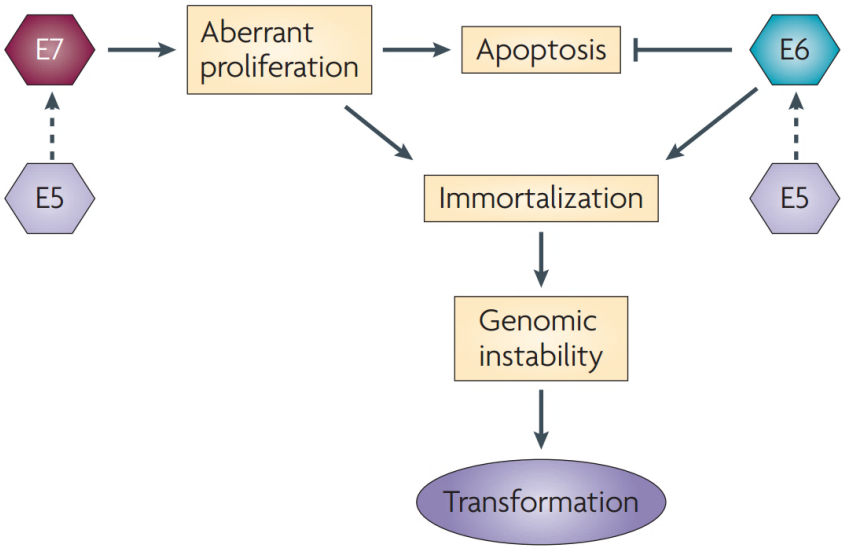

Figure 6: Collaboration of E5, E6 and E7 leading to malignant transformation. E5 stimulates expression of the other two oncogenes. E6 and E7 drive cellular processes towards cancerous transformation and simultaneously inhibit apoptosis. (Illustration adapted from [25])

E7 causes aberrant proliferation by E2F release and p21 inhibition leading in S-phase conversion. This considerable interference in cell cycle progression leads towards apoptosis by p53 accumulation [47]. However, E6 inhibits apoptosis by counteracting this process via p53 poly-ubiquitination and proteasomal degradation. The main contribution to cellular immortalization is the E6 mediated hTERT activation. However, E7 was shown to independently elongate telomeres via alternative lengthening [48, 49]. This dual mechanism might play a role in different HPV genotypes. Since the genetic constitution differs among HPV strains, this model possibly displays a backup for insufficient immortalization potential of either oncogene. Further progression towards malignancy is based on genomic instability. Both oncogenes induce aberrant mitosis, for instance resulting in centrosome abnormalities and aneuploidies [50]. Also either oncogene affects genomic instability at different time points. E6 mediates slow aberration, whereas E7 rapidly induces centrosome abnormalities [51]. These chromosomal aberrations usually induce apoptosis at the G_2-M checkpoint. The main function of the G_2-M checkpoint is prevention of cell cycle progression when DNA is damaged. Therefore, this checkpoint plays an important role in maintenance of genomic stability. The cellular p53 level is important for this checkpoint. The main function of p53 during this checkpoint is the inhibition of Cdk2 (Cyclin-dependent kinase 2) expression, which is the main contributor towards mitosis [52]. By p53 degradation the G_2-M checkpoint is bypassed and in addition E6 and E7 interfere apoptotic signaling [53]. However, the precise function of p53 in initial arrest and during long-term preservation of cellular stalling is not entirely understood [52]. The relevance of E5 in aberrational cell growth is mainly the enhancement of E6 and E7 expression [54, 55]. Although, the cancerous transforming effect of E5 was shown in specific circumstances [56].

Taken together E6 and E7 affect different cellular processes, which on their own may promote towards transformation. Nevertheless, the full potential in cellular progression

contributing to aberrant growth is the joint performance of both oncogenes with the support of E5.

1.3.3 Immune recognition of HPV

Immune recognition of HPV in the squamous epithelium of the cervix can be mediated by either the epidermis or the dermis. The main cell population of the epidermis is made up by keratinocytes, which conduct immune functionality, although they are no legitimate immune cells. Keratinocytes are able to present foreign antigen via MHC class I or, if expressed, MHC class II and secrete pro-inflammatory cytokines, without being professional antigen presenting cells (APC). In addition, professional APCs in the form of Langerhans cells and T cells are also located in the epidermal cell layer. The dermal repertoire of myeloid and lymphatic immune cells consists of a broader range. For induction of an adaptive immunity mainly Dendritic cells, NKT cells, B cells and T cells are located dermal. Whereby the T cell fraction is notably larger compared to the concentration in the blood and has substantial function in epithelial immunity [57].

In case of a HPV encounter the immune recognition is mainly mediated by epithelial recognition of viral pathogen associated molecular patterns (PAMP) and cellular damage associated molecular patterns (DAMP). Both stimuli lead to a Pattern-Recognition Receptor mediated activation of innate immune cells and initiate inflammation. Thus, pro-inflammatory neutrophils, macrophages and T cells are recruited and migrate towards the site of inflammation [58]. In addition to the typical immune recruitment the HPV risk-type seems to have an effect on that process. In high risk HPV infections the level of neutrophils and lymphocytes is elevated compared to low risk HPV and healthy squamous epithelium [59].

On the molecular level, HPV is potentially recognized via its circular dsDNA genome and its capsid proteins L1 and L2 [60]. After the viral invasion, endosomal Toll-like receptors and RIG-1-like receptors recognize HPV associated nucleic acids. In downstream signaling, the transcription factor Interferon-regulatory-factor 3 (IRF3) is activated, initiating the translation and export of Interferon-β (IFN-β). The surrounding cells are sensitive for released IFN-β and detect it via Interferon-α/β receptor (IFNAR). Thus, JAK-STAT-signaling and subsequently the formation of Interferon-stimulated gene factor 3 (ISGF3) is enabled, inducing expression of Interferon-stimulated genes (ISGs) by ISGF3 binding to the Interferon stimulated response element (ISRE). This enables the antiviral state in the affected region by expression of viral replication inhibitors, increased MHC I expression and enhanced sensitivity for apoptotic stimuli [61]. Thus, the infected site suppresses viral spread and recruits immune cells for eventual clearance.

1.3.4 HPV mediated immune evasion

Besides the immune recognition of HPV, the virus itself developed strategies to counter the immune response and interferes in cellular pathways. The intrinsic ability to oppose viral clearance is directly related to the persistence rate and seems also to be linked to high risk HPV genotypes [59].
The main contributors of immune evasion are E6 and E7. In general both viral proteins compromise innate immune response at several steps of the antiviral state induction. In detail, an essential step counteracted by HPV is IFN synthesis and signaling. The E6 protein affects the IFNAR and JAK-STAT mediated signaling by binding to the cytoplasmic domain of the IFNAR [62]. Thereby the receptor mediated phosphorylation and activation of the JAK-STAT pathway is impaired. E7 was shown to down-regulate IFN expression by preventing ISGF-3 complex formation [63]. Furthermore, E7 is able to prevent chromatin relaxation at the IFN-β promotor by inhibition of Histone acetyltransferases recruitment [64]. Thus, both oncoproteins affect antiviral state induction at different stages, but jointly contribute towards antiviral state prevention. HPV was also shown to ease the keratinocyte mediated activation of tissue residing immune cells and recruitment of T cells [65]. Therefore, HPV down-regulates the expression of various pro-inflammatory and chemotactic cytokines immediately after the infection [66].

1.4 Circulating tumor cells

Circulating tumor cells (CTC) were first described by Thomas Ashworth in 1869. He postulated a direct association of circulating tumor cells to an invasive tumor growth in invasive metastatic cancer [67, 68]. Twenty years after the first discovery, Stephen Paget published the ‘seed and soil’ hypothesis, which comprises the theory that metastases do not emerge by chance, but rather are the product of a particular tumor cell (‘seed’) establishing their growth in a definite tissue environment (‘soil’) [69]. This presumed relation was confirmed (among others) by Fehm, Sagalowsky [70]. In their study, they examined the chromosomal aberration in Cytokeratin pre-enriched CTCs and compared them to the primary tumor site. In the 31 patients included in the study, they found a variety of chromosomal aberrations. More interestingly in 10 out of 13 patients, biopsy material of the primary tumor was available and showed matching aneusomic chromosomal pattern when compared to that of CTCs [70]. This direct matching was verified in several cancer entities like breast, kidney, colon and prostate cancer patients, demonstrating its general importance. These findings directly feature the theory, in which detached cells of the primary tumor migrate via the blood stream and settle in secondary organs leading to metastasis.
The development of distant metastases mainly depends on breakdown of the epithelial layer in the primary tumor, circulation in the blood and migration into secondary tumor tissue (figure 7).

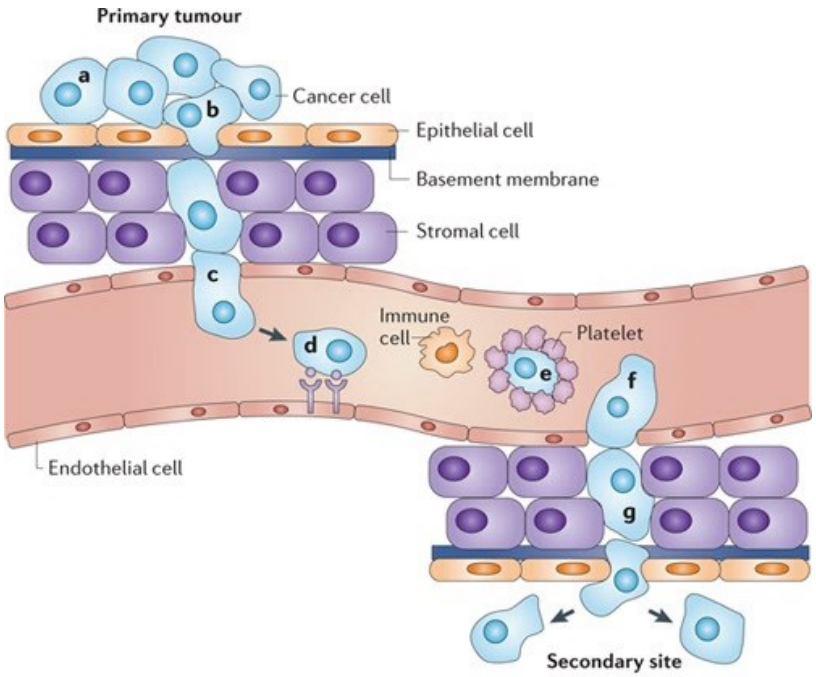

Figure 7: Metastatic spread of primary off-scaled cancerous cells (CTCs). Proliferating cells (a) in the primary tumor may start (b) breaking the epithelial barrier and migrate across the stroma. Scattered cells (c) overcome the vascular cell barrier. After release in the bloodstream the circulating tumor cells may (d) attach to receptors or (e) get bound by surrounding plates, which masks them and prevents immune recognition. At certain sites (f) CTCs can leave the blood stream and (g) remigrate into secondary tissue. (Illustration adapted from [71])

During the initial cellular aberration and tumor formation, many different cellular subpopulations emerge, varying in their biological and metastatic capability [72]. Out of this heterogenic aggregate, only few cells carry the ability to transit in the bloodstream and become pro-metastatic CTCs. In early progression of metastatic neoplasia a progressive growth can be observed, which is often associated with induced angiogenesis [5]. After successful establishment in the host tissue, invasive growth across the epithelial barrier into the stroma takes place. At this point capable tumor cells may enter circulating vessels. For this invasion the thin-walled lymphatic vessels are often utilized, since their endothelial cells provide little resistance [71]. After exiting the lymphatic system and entering the blood stream, most CTCs are being rapidly targeted and destroyed by immune cells [5]. In quantification experiments only 0.1% of all induces CTCs survived the first 24 hours and only 0.01% retained their metastatic ability [73]. One way of preventing immune recognition is for example platelets coating of CTCs. This envelope seems to even support further tumor metastasis development [74]. Furthermore, during circulation altered CTC gene expression may lead to epithelial-mesenchymal transition (EMT) and change the cellular fate [75]. During this process epithelial derived CTCs down-regulate characteristic epithelial markers like epithelial cell adhesion molecule (EpCAM) and Cytokeratins, which in general facilitates metastasis. While circulating, CTCs can be trapped by endothelial exposed receptors or the subendothelial membrane in branching capillaries [71]. In a next step, captured CTCs extravasate into the arrested organ by vascular remodeling or by barrier collapse [76, 77]. Subsequently, the implanted cell develops a

microenvironment and alienates surrounding cells to produce pro-inflammatory cytokines and growth factors [78]. Thus, metastatic establishment and progress is promoted.

1.4.1 Clinical relevance

Nowadays, the critical role of CTCs as precursors of metastasis is widely recognized and CTC detection and characterization is used as prognostic and predictive marker in several cancer entities like breast, ovarian, prostate, lung and colorectal cancer [79-82]. In the more than 90% of all cancer cases, patients die from the metastatic impact by affecting the functionality of an organ or eroding bones, rather than by the primary tumor disease [83, 84]. On the basis of these facts, the development of different approaches for CTC detection, quantification and isolation proceed over the past few years, aiming for the assessment of clinical utility [85]. The isolation of CTCs poses a substantial challenge, since quantities of 1 to 5 CTCs in 7.5 ml blood are of general case in early tumor stages or beginning metastatic relapse [68]. Clinical studies in CTC research focus on epithelial marker classification and additionally investigate more robust characteristics like gene expression profiles [86]. Although, there is no direct correlation between cervical cancer CTCs and clinical prognosis published, the general opinion indicates worse therapy response with an increasing number of CTCs. However, the poor median overall survival rate of cervical cancer patients with distant metastases, of about 12 months, depicts the impact of CTC mediated metastatic spread on prognosis [87]. Furthermore, the possibility of micrometastases mediated relapse indicates the relevance of a possible additional screening method utilizing CTCs for relapse monitoring.
There exist only a few publications, dealing with the characterization and detection of cervical cancer derived CTCs. Obermayr, Sanchez-Cabo [86] in their study focused on CTC marker identification and found a significant elevation of Cyclin E2 in 40% of the cervical cancer cell lines. Pfitzner, Schroder [88] published a digital-direct-RT-PCR approach for cervical cancer CTC quantification, which is based on the viral E6 gene. Applying this approach, they were able to detect CTCs in 3/10 (30%) cervical cancer patients of a selected cohort. However, until now an immunofluorescence staining based detection of cervical cancer derived CTCs is not described.

1.4.2 Cellular markers

For the CTCs enrichment and detection several different methods emerged over the recent years. These techniques are utilizing CTC specific characteristics like enlarged cellular size, lower plasticity, density or antigen dependent identification [89]. The most common route in CTC research is a combination of cell-attribute based pre-enrichment followed by antigen detection [90].

For this study, cervical cancer derived CTCs are pre-enriched by density gradient centrifugation and detected on the basis of the following cellular markers. Thereby, the epithelial character of this cancer, as well as the almost absolute abundance of an HPV infection was considered in the selection of suitable markers.

1.4.2.1 EpCAM

The epithelial cell adhesion molecule (EpCAM, CD326) is a surface glycoprotein encoded by the *EpCAM* or *GA733-2* gene locus located on chromosome 2 [91]. EpCAM is primarily expressed on basolateral surface and acts as a physical hemophilic interaction molecule [92]. The main function involves homophilic calcium-independent cell-cell adhesion and signal transduction [92]. During the cancerous-dedifferentiation EpCAM is known to be strongly overexpressed, making it a reliable diagnostic and CTC marker, especially since it is not expressed in hematopoietic cells [86, 93]. Although, its direct contribution to carcinogenesis remains unclear, but the role in tumor progression and metastases formation seems essential in most tumors [94, 95]. Albeit, the EpCAM expression level diminishes during circulation and may ease over time by EMT [75]. In the progression of cervical cancer the EpCAM-negative squamous cervical epithelia is also reported to initiate EpCAM expression concomitant with its transformation [95]. Hence, its importance in cancerous progression and metastasis, EpCAM is a clear CTC marker indicating epithelial origin.

1.4.2.2 Cytokeratins

Cytokeratins (nowadays named Keratins) are a heterogeneous group of keratin-containing intermediate filaments, divided into basic type I and acidic or neutral type II Keratins [96]. The monomers of these fibrous structural proteins are bundling to high molecular filaments forming mammalian tissue scaffold, which are for example involved in the development of high-molecular formations like hair or nails. However, several cytokeratins are also known to be cancer related. In particular cytokeratin 19 is known as a general carcinoma marker, cytokeratins 8 and 18 are proven as specific markers for adenocarcinomas such as cervical carcinoma [97-99]. Thus, Cytokeratin expressing cells in the peripheral blood can be classified as cancer derived.

1.4.2.3 Cyclin E2

G1/S-specific Cyclin E2 is a member of the Cyclin protein family and encoded by the *CCNE2* gene locus located on chromosome 8 [100]. During cell cycle progression, at the end of G_1-phase, Cyclin E2 complexes with Cdk2 (Cyclin-dependent kinase 2) promoting the cellular G_1-S-phase transition [101]. The expression of Cyclin E2 initiates mid-G_1 and is a rate-limiting factor for the passage through G_1-phase [102]. HPV E7 was shown to indirectly facilitate the cellular Cyclin E2 level due to RB phosphorylation and subsequent E2F activation. The released and activated E2F binds to the *CCNE2* promotorsite and enhances the Cyclin E2 expression, resulting in an auto-regulatory

loop [103]. Moreover, HPV E7 directly associates with cellular Cyclin E2 [104], contributing an additional mechanism of cellular hyperproliferation. Aberrant Cyclin E2 overexpression was demonstrated for CINs and cervical cancer [105]. Furthermore an elevated expression in cervical cancer derived CTCs was shown in other studies [86]. Therefore, Cyclin E2 serves as a surrogate cervical cancer marker, validating the cellular CTC state.

1.4.2.4 Cyclin-dependent kinase inhibitor 2A

Cyclin-dependent kinase inhibitor 2A or p16-INK4a (p16) is a tumor-suppressor gene and selective Cyclin-dependent kinase inhibitor. p16 is encoded by the *CDKN2A* gene locus located on chromosome 9 [106]. During cell cycle progression p16 binds to cdk4 and cdk6 inhibiting the RB phosphorylation, resulting in the maintenance of the RB-E2F complex [107]. Since HPV E7 mediates the RB phosphorylation and subsequently the release of the RB-E2F complex, the cell counteracts by increased p16 expression. Furthermore, elevated expression during cancer progression was shown to be accurate with increasing evidence from CIN I to squamous cell carcinoma [108]. Thereby the overexpression of p16 in CIN and cervical cancer serves as surrogate marker for HPV E7 mediated pRB catabolism [107, 109]. Moreover, p16 overexpression by circulating cells can be seen as a specific and indirect marker for HPV E7 [107].

1.4.2.5 Receptor-type tyrosine-protein phosphatase C

Cluster of differentiation 45 (CD45) or PTPRC, former leukocyte common antigen (LCA), is encoded by the *PTPRC* gene located on chromosome 1. CD 45 is classified as Protein tyrosine phosphatase (EC number 3.1.3.48) and required for T cell activation [110]. Due to the expression in all nucleated hematopoietic cells, antibodies against CD45 are used as pan-immune cell marker [111]. Therefore, CD45 is used as discrimination of epithelial CTCs from mononuclear leukocytes.

1.5 Working hypothesis

The general detection of epithelial cancer derived CTCs is mainly based on the detection of characteristic epithelial tissue markers, similar to EpCAM and Cytokeratin, and well described in the literature. However, the reliability of these markers is directly associated with EMT and leads to narrowed detectability over time. In the particular case of cervical cancer, no established immunofluorescence based CTC detection is mentioned in the literature. To achieve this objective, HPV derived proteins, as CTC marker, offer the opportunity to directly specify the origin of detected CTCs. The deployment of recently developed anti-HPV E7 antibodies could contribute to such an approach. Besides direct detection of viral proteins, also HPV-altered cellular processes provide surrogate markers.

Therefore, we hypothesized that cervical cancer derived CTCs are detectable by a five-color immunofluorescence staining via: 1) the general epithelial cancer markers Ep-CAM and Cytokeratin, 2) the essential viral protein E7 and 3) the surrogate markers for aberrant cellular growth Cyclin E2 and p16.

1.6 Aim of this study

The aim of this study was the establishment of a marker panel for the antigen based identification of cervical cancer derived CTCs in the peripheral blood through a five-color immunofluorescence staining. This approach might later on serve as a tool for cervical cancer relapse monitoring. In that course, established epithelial CTC markers, described in the literature, a novel direct HPV marker and HPV surrogate markers were utilized for CTC detection. Due to the dominant position in clinical cervical cancer cases, only the high risk HPV genotypes HPV16 and HPV18 are considered in this study. Furthermore, a computer-based image evaluation and CTC detection should be established to contribute and facilitate the screening process.

2 Material and methods

2.1 Cervical cancer derived CTC detection

2.1.1 Study population and patients‘ material

Blood from 59 female patients with diagnosed cervical cancer and blood of two healthy controls was collected between August 2012 and September 2014 at the Department of Obstetrics and Gynecology of the Medical University of Vienna, Austria. Patients' blood samples were collected at the time of primary diagnosis. All included patients signed an informed consent for the use of blood and tissue in the study. The study was approved by the local ethics committee.

2.1.2 Blood sample collection and processing

4 x 9 ml of peripheral blood was collected at the time of primary diagnosis. Blood samples were drawn in Vacuette® EDTA tubes and processed within 2 h.
Density gradient centrifugation of whole blood was performed according to a protocol published by Brandt et.al, to receive a so called ‘CTC enriched fraction’ [112]. Therefore 6x 15 ml polystyrene tubes were primed with 10 ml saturation solution containing 1% FCS in PBS. The density gradient consisted of 3 ml PolymorphPrep™ (d = 1.113 kg/l, osmolality = 445 mOsm) and 3 ml NycoPrep 1.068 (d = 1.068 kg/l, osmolality = 335 mOsm), carefully overlaid with 5 ml of EDTA whole blood. Samples were centrifuged at 450 g for 20 min with disabled break. Centrifugation separated the whole blood in plasma, CTC enriched / Peripheral blood mononuclear cell (PBMC) fraction and granulocyte fraction (figure 8). 3 ml of the CTC enriched fraction were collected in a 50 ml equilibrated polystyrene tube. Cells were washed once with PBS and centrifuged at 200 g for 10 min. The pellet was resuspended in 10 ml PBS, half of the solution was washed a second time in 50 ml PBS and centrifuged at 200 g for 10 min. The processed cells were resuspended in 10 ml PBS.

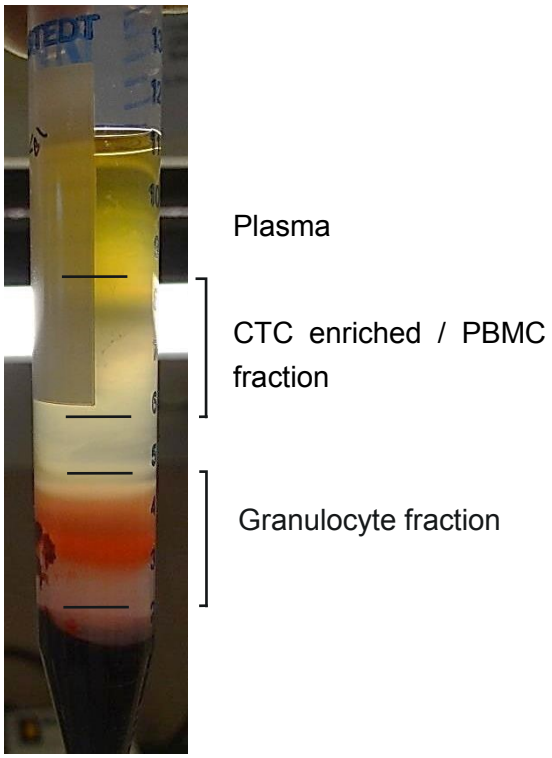

Figure 8: Typical appearance of whole blood after density gradient centrifugation. The blood sample is separated in the three fractions: plasma, CTC-enriched / PBMC and the granulocytes.

2.1.3 Cytospin

For cytospin preparation of the CTC enriched fraction, 1.25 ml of the cell suspension was applied onto Polysine™ Microscope Adhesion Slides (Thermo Scientific, USA) and MembraneSlides (Molecular Machines & Industries, Germany) each, corresponding to cells of 4.5 ml of whole blood / slide. Slides were centrifuged at 160g for 5 min.

2.1.4 Cell culture

The cervical cancer cell lines Ca Ski (ATCC® CRL-1550™) and ME-180 (ATCC® HTB-33™) were cultivated in RPMI medium (Thermo Scientific, USA) containing 10% FCS (Thermo Scientific, USA) and 1% Penicillin Streptomycin (Thermo Scientific, USA) to 90% harvesting confluence. Cells were harvested, washed two times with PBS and centrifuged at 1,000 rpm for 10 min. The resulting cells were resuspended in 2 ml PBS and used for preparation of cytospins, as positive control for the immunofluorescence stainings.

2.1.5 Staining controls

Panel 1 antibody elaboration and staining controls were done using the HPV16 positive cell line Ca Ski. For the second panel, the HPV18 positive cell line ME-180 was utilized. Both diverging cell lines were established from metastases, which derived from epithelial cervical cancer. These cell lines were selected in coordination with cellular

marker specific antibodies, which are known to exhibit an antigen specific signal using either cell line. For positive control preparation, the PBMC fraction of a healthy donor was either spiked with $1x10^4$ Ca Ski or $1x10^4$ ME-180 cells. As negative control, exclusively the PBMC fraction of a healthy donor was utilized. All staining control cytospins were produced at the same time point, avoiding cell culture dependent differences.
Simultaneously to all immunofluorescence stainings, positive and negative controls were performed according to the staining procedure (see chapter 2.1.6.2). The positive control serves as a validity control and verifies the general experimental staining success. Positive staining controls of either panel should result in CTC marker specific indication of both cell lines without comprising a CD45 signal, whereas the PBMCs should be exclusively positive for CD45. Performed negative controls ensure no cross-reactivity of the CTC marker specific antibodies on PBMCs. Therefore, the PBMCs should also only exhibit CD45 staining.

2.1.6 Immunofluorescence staining

2.1.6.1 Antibodies

A set of eight different primary antibodies was used for multicolor indirect immunofluorescence staining. For each panel four different primary antibodies obtained from different species, isotypes and clonality were used for multiple staining of single cells. In panel 1 the following primary antibodies were used: monoclonal anti-human CD45 (1:1000, host rat, isotype, IgG2b, clone orb96558, biorbyt, United Kingdom), monoclonal pan-anti-cytokeratin 8, 18, 19 (1:100, host mouse, IgG1, clone A45-B/B3, AA Diagnostik, Germany), polyclonal anti-EpCAM (1:200, host rabbit, IgG, catalog number 21050-1-AP, proteintech, USA) and monoclonal anti-HPV16/31 E7 (1:300, host mouse, IgG2a, catalog number VS13008, Valdospan, Austria). Panel 2 consists of: monoclonal anti-human CD45 (1:1000, host rat, isotype, IgG2b, clone orb96558, biorbyt, United Kingdom), polyclonal anti-Cyclin E2 (1:200, host rabbit, IgG, catalog number 11935-1-AP, proteintech, USA), monoclonal anti-CDKN2A/p14ARF (1:400, host mouse, IgG2a, clone ARF 4C6/4, abcam United Kingdom) and monoclonal pan-anti-cytokeratin 8, 18, 19 (1:500, host mouse, IgG1, clone 2A4, Enzo, Austria). In addition the non-commercially available monoclonal anti-HPV18/45 E7 (1:500, host mouse, IgG1, clone 177-121-1, VALDOSPAN Austria) antibody was tested during panel 2 assortment. The secondary antibodies were directed against the species and isotype of corresponding primary antibody and carried a fluorescent tag. The utilized secondary antibodies for panel 1 are: anti-rabbit IgG Alexa Fluor® 488 conjugate (1:1000, whole antibody, Invitrogen, Life Technologies, USA), goat anti-Mouse IgG2a Alexa Fluor® 555 conjugate (1:1000, whole antibody, Invitrogen, Life Technologies, USA), Goat anti-Rat IgG (H+L) Alexa Fluor® 594 conjugate (1:1000, whole antibody, Invitrogen, Life Technologies, USA), goat anti-Mouse IgG1 Alexa Fluor® 647 conjugate (1:1000, whole antibody, Invitrogen, Life Technologies, USA). Panel 2 consists of: anti-

rabbit IgG Alexa Fluor® 488 conjugate (1:1000, whole antibody, Invitrogen, Life Technologies, USA), goat anti-Mouse IgG2a Alexa Fluor® 555 conjugate (1:1000, whole antibody, Invitrogen, Life Technologies, USA), goat anti-Mouse IgG1 Alexa Fluor® 594 conjugate (1:1000, whole antibody, Invitrogen, Life Technologies, USA), goat anti-Rat IgG Alexa Fluor® 647 conjugate (1:1000, whole antibody, Invitrogen, Life Technologies, USA). All appropriate primary antibody dilutions were determined in dilution experiments. For these trails, slides, prepared according to chapter 2.1.5, were stained with a decreasing antibody dilution. Dilutions were settled to a reliable CTC detection in the positive control, without producing any background in the negative control. Secondary antibodies were utilized according to manufacturer's information. The allocation of primary antigens to the corresponding fluorescence channels can be seen in table 2:

Table 2: Antigen-panel composition. Assignment of fluorescence labeled secondary antibodies to corresponding antigens in panel 1 and 2.

Dye	Panel 1	Panel 2
Alexa Fluor® 488	EpCAM	Cyclin E2
Alexa Fluor® 555	HPV16 E7	p16
Alexa Fluor® 594	CD45	Cytokeratin 8,18,19
Alexa Fluor® 647	Cytokeratin 8,18,19	CD45

The composition of the secondary antibodies was chosen according to their fluorescent dye and the capabilities of the confocal laser scanning microscope, for minimal overlap of the emission spectra (figure 9).

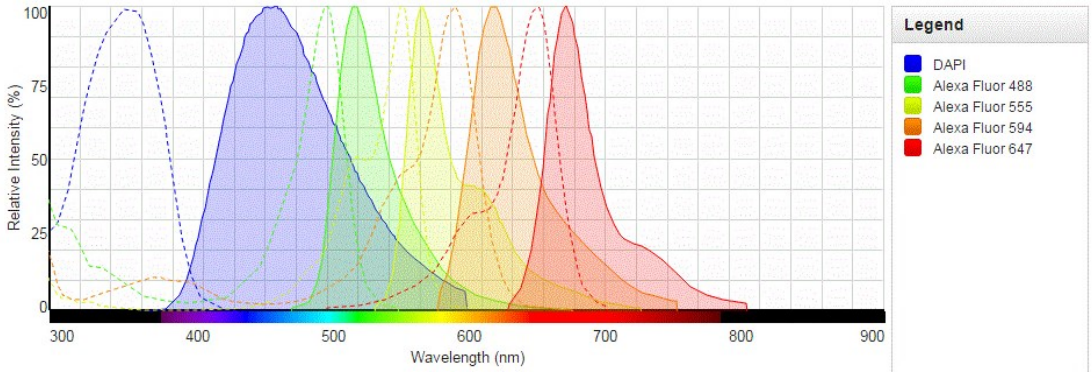

Figure 9: Excitation and emission spectra of utilized secondary antibodies. Excitation (dotted line) and emission (solid line) spectra of fluorophores linked to secondary antibodies. (Illustration obtained from http://www.lifetechnologies.com/at/en/home/life-science/cell-analysis/labeling-chemistry/fluorescence-spectraviewer.html, 13.03.2015)

2.1.6.2 Staining procedure

For multi-color secondary immunofluorescence staining, patients' cytospins were first fixed using 4% paraformaldehyde for 10 min at RT. Slides were washed 3 times using PBS for 4 min each. Cellular permeabilization was achieved by incubating the slides for

10 min in 0.5% Triton X (0.5% Triton X in PBS) at RT. Subsequently cytospins were washed 3 times using PBS for 4 min each, blocked using Lab Vision™ Ultra V Block (Thermo Scientific, USA) for 7 min and rinsed with Milli-Q™ water. Superfluous liquid was removed and the set of appropriate diluted primary antibodies, using Antibody Diluent (Dako, USA), was applied at 4°C over night. After washing the slides 3 times with 0.1% Tween® 20 (0.1% Tween® 20 in PBS) for 3 min, the appropriate secondary antibodies, diluted in 6% BSA, were applied onto the cytospins for 60 min at RT. The cytospins were subsequently washed 3 times in PBS for 3 min and the nuclei were stained using 50 ng / ml DAPI for 5 min. Subsequently slides were rinsed with Milli-Q™ water and mounted with Fluoromount-GTM (Southern Biothech, USA).

2.1.7 Microscopy and image evaluation

2.1.7.1 TissueFAXS

The StrataFAXS system (TissueGnostics, Austria) was used for fluorescence acquisition of the cytospins surface. All images were acquired using the EC Plan-Neofluar 20x/0.50 M27 objective (Carl Zeiss, Germany) with the following excitation filters DAPI (365 nm, bandwidth 30nm), FITC (485nm, bandwidth 20 nm), Texas Red (560nm, bandwidth 40 nm) and Cy5 (645nm, bandwidth 30 nm). As light source the mercury-vapor system X-Cite® 120PC (Excelitas Technologies, USA) was used with a channel specific excitation time of DAPI, FITC, Texas Red and Cy5. Images were acquired using the ORCA-Flash4.0 V2 digital camera (Hamamatsu Photonics, Japan). TissueFAXS Viewer (version 4.2, TissueGnostics, Austria) was utilized for computational consideration.

2.1.7.2 Confocal laser scanning microscopy

Slides were imaged using the LSM 780 (Carl Zeiss, Germany) microscope. For excitation the following lasers Diode Laser 405nm, Multiline Argon laser 458/488/514nm, Diode Laser 594nm and Helium-Neon laser 633nm with the according main beam splitter MBS-405, MBS-488/561/633, MBS-458/514, MBS-488/594 were adjusted for minimal emission overlay. Acquisition of all pictures was done using either the Plan-Apochromat 20x/0.8 M27 (Carl Zeiss, Germany) or Plan-Apochromat 63x/1.40 Oil DIC objective (Carl Zeiss, Germany). To minimize the overlap of the different secondary antibodies the detection channels were truncated according to table 3.

Table 3: Wavelength setup for confocal laser scanning microscopy. Setup was chosen for minimized fluorescence emission overlay.

Dye	Panel 1	Panel 2
DAPI	410-486nm	410-486nm
Alexa Fluor® 488	488-550nm	488-550nm
Alexa Fluor® 555	550-586nm	550-586nm
Alexa Fluor® 594	599-649nm	580-629nm
Alexa Fluor® 647	649-758nm	664-757nm

All obtained fluorescence images were stored as lsm-files (resolution 2048x2048, 8bit depth, scan time 6, unidirectional). Consideration and downstream analysis was done using IMARIS (version 7.4.2, Bitplane, United Kingdom).

2.1.7.3 CTC identification

For manual CTC identification, the TissueFAXS images were manually evaluated. Cells exhibiting a considerable staining for at least one CTC marker were retained and, for a more detailed analysis, visualized using the CLSM.
For automated CTC quantification, the obtained TissueFAXS images were processed using a CellProfiler (version 2.1.1, Broad Institute, USA) pipeline [113]. The developed image analysis consists of cellular differentiation (including nucleus-cytoplasm distinction), several graphical improvements for background reduction, cellular staining enhancements and fluorescent amplification. Subsequently, the CTC specific channels were merged and overlapping fluorescence was matched to the immune cell channel. The cutoff-definition for the $CD45^+$ population was set according to staining in negative control samples. For the CTC specific channels the cutoff was set according to the positive control values.

2.2 FFPE based HPV genotyping

In addition to the immunofluorescence based CTC detection, the opportunity of a HPV dependent gene expression-based CTC detection, utilizing the available patient material, should be elaborated. For this purpose, a HPV genotyping protocol, routinely used for the analysis of Pap-smear samples, should be tested for its applicability on available FFPE material. On this basis, the validity of the prospective gene expression-based CTC detection might be examined.

2.2.1 Study population and patients‘ material

Cervical Pap-smears and cervical biopsies of 7 female patients with diagnosed CIN I-III were collected between April 2010 and March 2011 at the Department of Obstetrics and Gynecology of the Medical University of Vienna, Austria. All included patients

signed an informed consent for the use of cervical Pap-smears and tissue in the study. The HPV genotype of all Pap-smear samples was available. The study was approved by the local ethics committee.

2.2.2 Cell culture

The cervical cancer cell line SiHa (ATCC® HTB-35™) was cultivated in RPMI medium (Thermo Scientific, USA) containing 10% FCS (Thermo Scientific, USA) and 1% Penicillin Streptomycin (Thermo Scientific, USA) to 90% harvesting confluence. Cells were harvested, washed two times with PBS and centrifuged at 1,000 rpm for 10 min. The resulting cells were resuspended in 2 ml PBS. 10 µl of the cell suspension was stained with 10 µl 0.4% Trypan Blue solution (Life Technologies, USA) and counted using Countess® Automated Cell Counter (Life Technologies, USA). As DNA extraction control (see chapter 2.2.3) $2.5x10^4$ SiHa cells / ml in PBS were prepared.

2.2.3 DNA extraction

Pap-smear samples were stored in Digene Hybrid Capture® transport media (Qiagen, Germany) at -20 °C. Isolation of the cellular DNA was achieved using the oCheck® DNA Extraction Kit (greiner bio-one, Austria), following the PapilloCheck® protocol. Prior to DNA extraction FFPE samples were deparaffinized by incubation in 1,000 µl or 500 µl xylene for 30 min at RT followed by centrifugation at 11,000 g for 3 min. The supernatant was aspirated and discarded. Remaining xylene was removed by adding 1 ml 96% ethanol, mixing by inverting several times and centrifugation at 11,000 g for 3 min. Supernatant was discarded and remaining ethanol was evaporated at 37 °C for 15 min. Deparaffinized samples were resuspended in 250 µl Milli-Q™ water. As extraction control two 250 µl aliquots of the $2.5x10^4$ SiHa cells / ml in PBS suspension were treated according to the FFPE protocol or the regular oCheck® extraction.

2.2.4 Genotyping

HPV genotyping of Pap-smear samples and CIN biopsies was done using PapilloCheck® (greiner bio-one, Austria). The PapilloCheck® PCR system compromises three different amplification systems, targeting the HPV E1 gene, the human Adenosine deaminase, tRNA-specific 1 (ADAT1) gene (as sample control) and an artificial plasmid (as general PCR control). Following the PCR, the amplified products are hybridized to genotype-specific DNA probes and labeled via a fluorescent tag. The DNA-array consists of 24 genotype-specific DNA probes, which facilitate the simultaneous detection of high-risk and low-risk HPV genotypes, each as fivefold replicates (depicted in figure 10). Subsequently, readout via laser excitation is generated, indicating the validity and genotype of the analyzed sample.

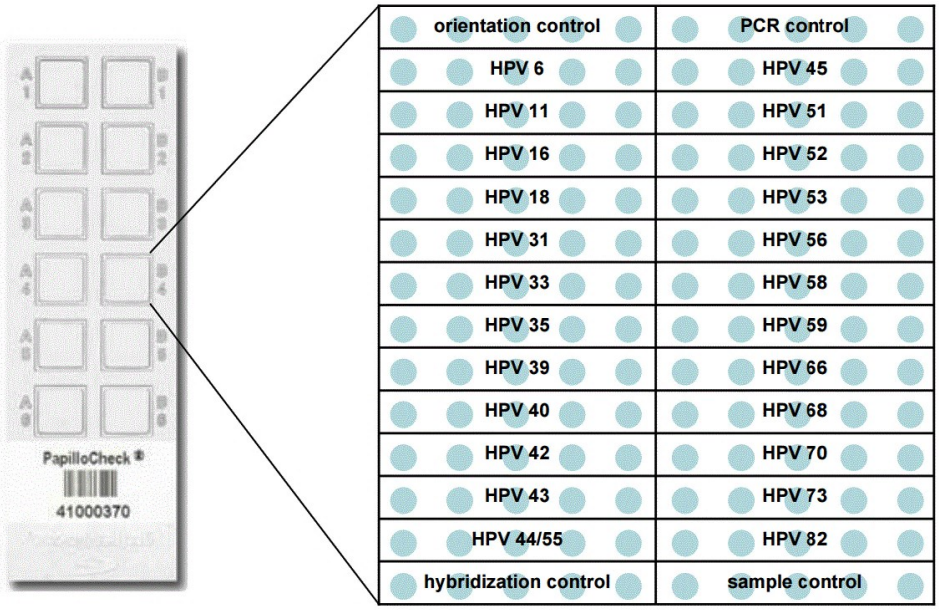

Figure 10: Scheme of the greiner bio-one PapilloCheck® DNA-hybridization array. Left: Hybridization slide, carrying twelve reaction arrays. Right: Singe reaction array. Circles indicate the hybridization sectors for control reactions and HPV-genotype specific hybridization. (Illustration obtained from: http://www.greinerbioone.com/UserFiles/File/English%20files%20for%20the%20UK%20website/Biochips%20pdf/Papillocheck%20manual%20May%202006.pdf, 16.03.2015)

3 Results

3.1 Overview

Blood samples of n=59 patients were included in the CTC detection study, collected between August 2012 and September 2014. The included patients were pathologically diagnosed with cervical cancer differing in FIGO stage and grade (table 4). Certain cervical cancer blood samples were obtained from external cooperation partners, lacking the specific stage and grade information.

For the HPV genotyping paired Pap-smear and FFPE biopsies of n=7 CIN patients were utilized. The samples were collected between April 2010 and March 2011. Pathologic diagnosis and classification of the FFPE samples was done during clinical routine procedure. Two patients were retrospectively excluded due to an insufficient sample amount and poor sample quality.

Table 4: Patient and tumor characteristics

Characteristics		CTC Detection Number of Patients (%) n=59	HPV Genotyping Number of Patients (%) n=7
Mean age at diagnosis		46.88 (SD 12.76)	29.71 (SD 6.78)
FIGO			
	IA	2(3.4)	
	IA1	2(3.4)	
	IB	5(8.5)	
	IB1	15(25.4)	
	IB2	5(8.5)	
	IIA	2(3.4)	
	IIB	18(30.5)	
	IIIB	3(5.1)	
	IV	1(1.7)	
	IVA	1(1.7)	
	IVB	1(1.7)	
	not specified	4(6.7)	
Grade			
	1	13(22.0)	
	2	18(30.5)	
	3	12(20.3)	
	not specified	16(27.2)	

CIN	
CIN 1	2(28.6)
CIN 2	3(42.8)
CIN 3	2(28.6)
HPV genotype	
16*	3(42.8)
31	1(14.3)
42	1(14.3)
53*	1(14.3)
59*	1(14.3)

* A single patient is triple-positive for the genotypes 16, 53 and 59

3.2 Cytospin processing

Patients' blood samples were processed according to the protocol (see chapter 2.1.6). In a number of cases the donated blood volume was lower than 30 ml. In these cases the regular blood volume of 5 ml per gradient was reduced and the available volume was equally allocated. An absolute volume of 1.25 ml of the CTC enriched fraction was utilized for cytospin processing. The cellular quantity was not determined and presumably differs between patient samples. Dried samples were stored at -20 °C until further processing.

3.3 Immunofluorescence based CTC detection

For CTC identification and characterization, the appropriate antibody concentrations were determined separately for each antibody. Suitable dilutions resulted in adequate antigen detectability, without comprising a background staining. All elaborated dilutions were repeatedly tested and the final working concentrations are depicted in table 5.

Table 5: Working concentrations of utilized antibodies

Antigen	Panel	Dilution
EpCAM	1	1:200
Cytokeratin	1	1:100
HPV16 E7	1	1:300
Cyclin E2	2	1:200
p16	2	1:400
Cytokeratin	2	1:500
CD45	1/2	1:1,000

The processed cytospins of cervical cancer patients were stained with antibodies targeting either EpCAM, HPV16 E7, pan-Cytokeratin and CD45 (panel 1) or Cyclin E2, p16, pan Cytokeratin and CD45 (panel 2). All cytospins were visualized by fluorescence microscopy (via TissueFAXS) and confocal laser scanning microscopy

(LSM 780). Parallel to patients' cytospins, positive and negative staining controls (prepared according to 2.1.5) were processed.

The overall evaluation of all stained cytospins resulted in 10/59 (16.9%) patients with detectable CTCs. The individual analysis of panel 1 and 2 yielded in 5/59 (8.5%) and 6/59 (10.2%) cases, respectively. In 1/59 (1.7%) patient both staining panels featured detectable CTCs.

3.3.1 TissueFAXS

Prepared cytospins were stained according to the protocol either with panel 1 or panel 2 standards. Exposure times for each channel were adapted to the control staining and followed the computer program suggested values. In all samples the whole surface area of the cytospins was scanned, resulting in approximately 30x30 fields of views (FOV), which corresponds to 1.44 cm^2. As focus strategy an automatically adapted strategy for an area of 3x3 FOVs was used.
In all samples the cell count per unit area differed among the processed samples and also within certain areas of one sample. It ranged from approximately 20 cells per FOV, in low dense areas, to more than 1,000 cells per FOV in areas of high density. For example in figure 11 the overall density, cell distribution and fluorescence intensity diverged among the individual samples. A frequent observation among almost all panel 1 slides was a very dense and intense green background staining, which was only present in the FITC filter. Moreover, some cytospins exhibited overlapping surface areas, which seemed to be detached during staining and back-folded in further processing (like 14528, depicted in figure 11). All three patterns of varying cell density, intense background staining and overlapping surfaces were not present in sample controls. Panel 2 cytospins were also affected by the varying cell density, although, detached or overlapped areas were not observed. The intense background fluorescence in the lower wavelength area remained consistent and did, in turn, not exist among the controls. In general, the TissueFAXS images were highly divers in staining intensity and overall processing quality. In addition, the used focus strategy resulted in minor focus variations, by which some obtained images were slightly blurry. Other than the mentioned issues, the predominant proportion of the tremendous image amount was acquired in appropriate quality, suitable for further CTC identification. The obtained images were evaluated and potential CTCs were identified by positive staining for the respective cervical cancer markers and the absence of immune cell marker CD45.

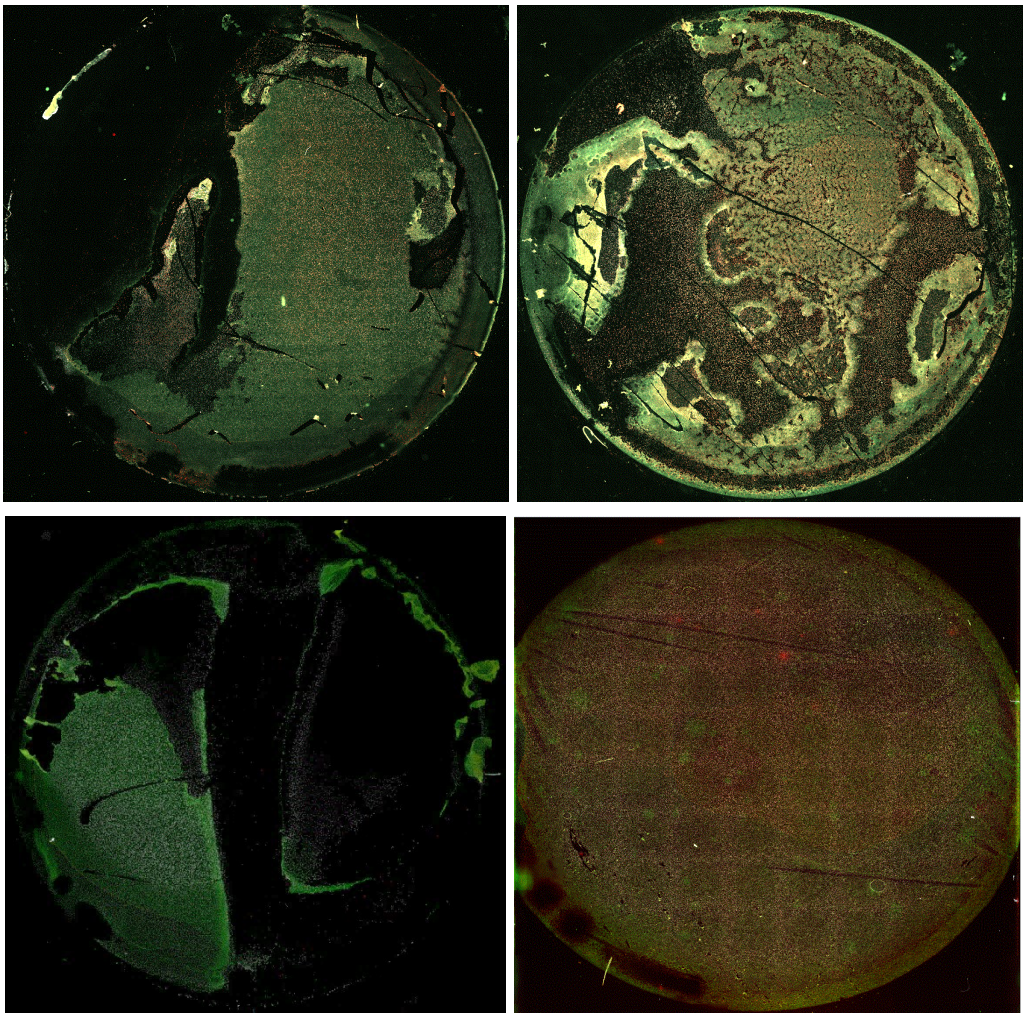

Figure 11: TissueFAXS overview of stained cytospins. Differences in captured fluorescence images (upper-left: patient 14528 - panel 1, upper-right patient 12588 - panel 1, lower-left patient 12588 - panel 2 and lower-right patient 15641 - panel 2). Approximate size: 30x30 FOVs or 1.44 cm^2.

3.3.2 Panel 1

Possible CTC containing areas, previously identified through a manual analysis of the images generated by the TissueFAXS, were captured using the CLSM. The wavelength setup for each fluorescence channel was adjusted to the control stainings (figure 25 and figure 26) and is depicted in table 3. Only cells, which show a fluorescence staining signal above a certain background, being identified as possible CTCs and thereby preventing the count of false positive cells. CTCs were defined as cells showing a nuclear (DAPI) staining, a reliable staining of at least one of the cervical cancer specific markers, and the absence of a CD45 signal. Applying the panel 1 staining, in 5/59 (8.5%) patients CTCs were identified, varying in specific marker positivity.
In sample 13288 three CTCs were identified. These cells were located nearby on the cytospin preparation (figure 12). The stained cells were $EpCAM^+$, HPV16 $E7^+$, $Cytokeratin^+$ and $CD45^-$. Also the specific fluorescence level was notably above the background. One of the CTCs exhibited an enlarged and aberrant nucleus, which additionally appeared to be allocated.

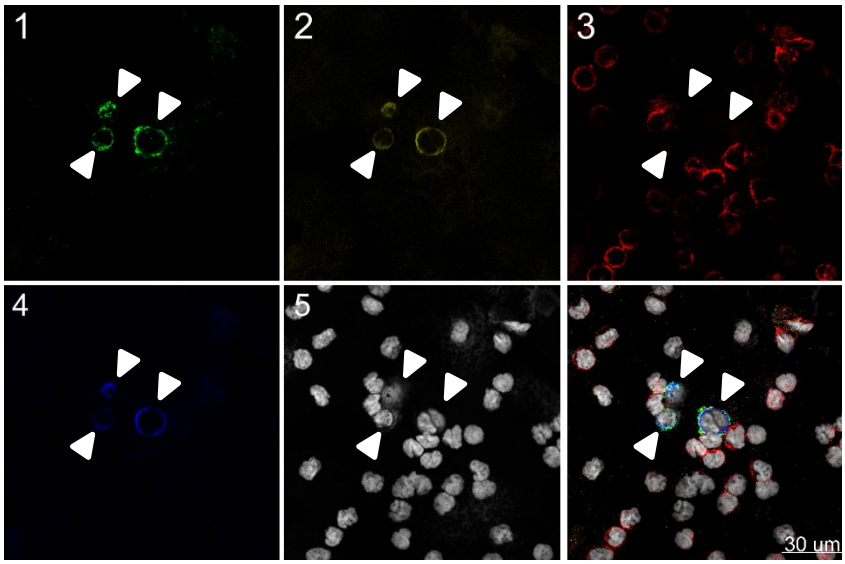

Figure 12: IF staining of patients' CTC (13288). (1) EpCAM – green, (2) HPV16 E7 – yellow, (3) CD45 – red, (4) pan Cytokeratin – blue, (5) DAPI – grey, (6) merge. Arrows indicating cervical cancer derived CTCs.

Sample 13625 revealed a very high total amount of twelve positive CTCs among the hematopoietic cells. In figure 13 six EpCAM$^+$, HPV16 E7$^+$, Cytokeratin$^+$ and CD45$^-$ cells are in close proximity. In contrast to EpCAM and Cytokeratin, the HPV E7 staining generated a slight background on CD45$^+$ cells. However, the HPV16 E7 signal was considerably stronger and more consistent in EpCAM$^+$ and Cytokeratin$^+$ cells. Furthermore, the nuclear size was slightly enlarged in relation to the immune cells.
Compared to sample 13288 the cellular location of all three CTC markers in patient 13625 seemed to be shifted towards the cytoplasm. This pattern was particularly strong in one distinct CTC (figure 13, indicated by the red arrow).

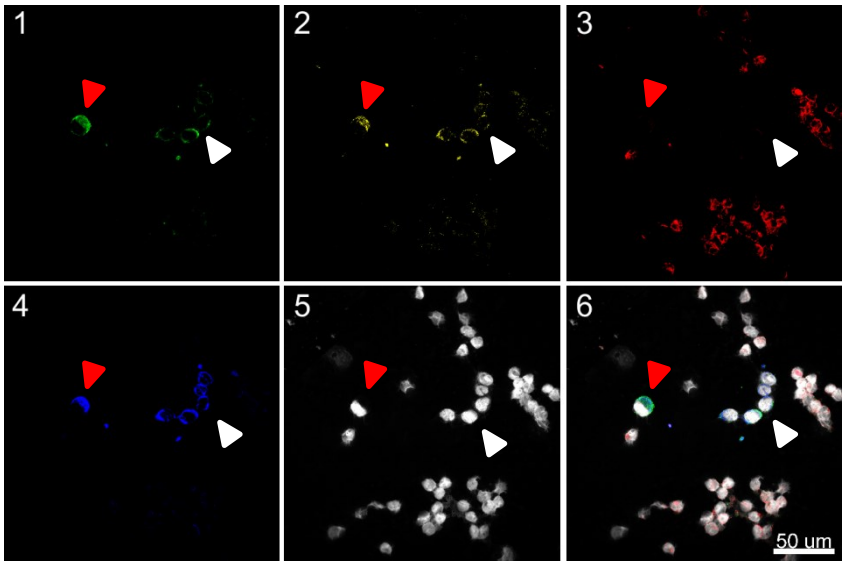

Figure 13: IF staining of patients' CTC (13625). (1) EpCAM – green, (2) HPV16 E7 – yellow, (3) CD45 – red, (4) pan Cytokeratin – blue, (5) DAPI – grey, (6) merge. Arrows indicating cervical cancer derived CTCs.

CTC staining of sample 14295 (figure 14) followed the pattern of positive panel 1 markers and was comparable to patient 13625. Both, the EpCAM and Cytokeratin stainings were conspicuous without background interference. The HPV16 E7 signal was less specific and resulted in a remarkably high background signal. However, the CTC specific HPV16 E7 signal was clearly above the background level. The CD45 staining also resulted in a less delimited staining with enhanced background noise. Looking at the DAPI channel, nuclei in different optical layers were distinguishable, possibly causing the elevated background fluorescence.

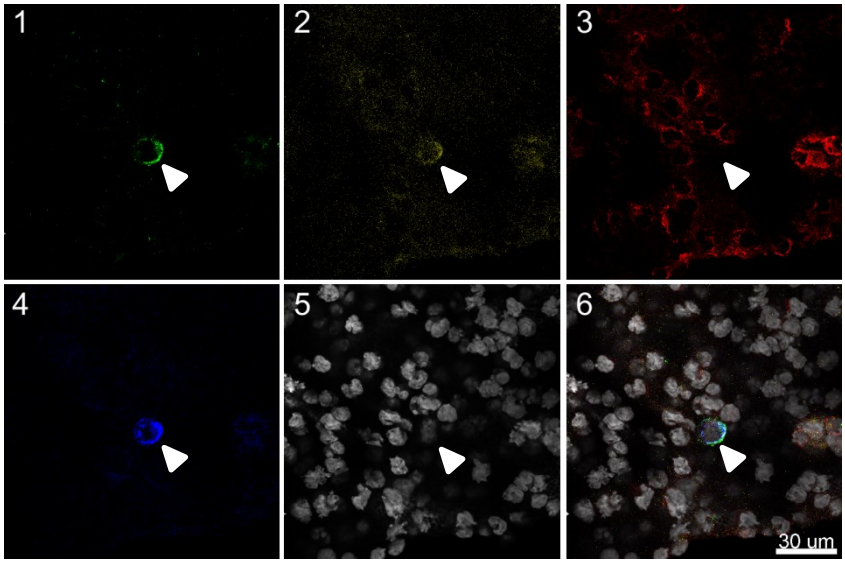

Figure 14: IF staining of patients‘ CTC (14295). (1) EpCAM – green, (2) HPV16 E7 – yellow, (3) CD45 – red, (4) pan Cytokeratin – blue, (5) DAPI – grey, (6) merge. Arrow indicates cervical cancer derived CTCs.

In contrast to the other panel 1 results, the sample 14095 and 14349 (figure 15 and figure 16, respectively) revealed inconsistent CTC stainings. The detected CTC in patient 14095 is $EpCAM^{+}$ and $Cytokeratin^{+}$, but lacks an explicit HPV16 E7 signal. Similar to patient 14295, the background staining in the HPV16 E7 and CD45 channels is elevated and cells are less delimited.

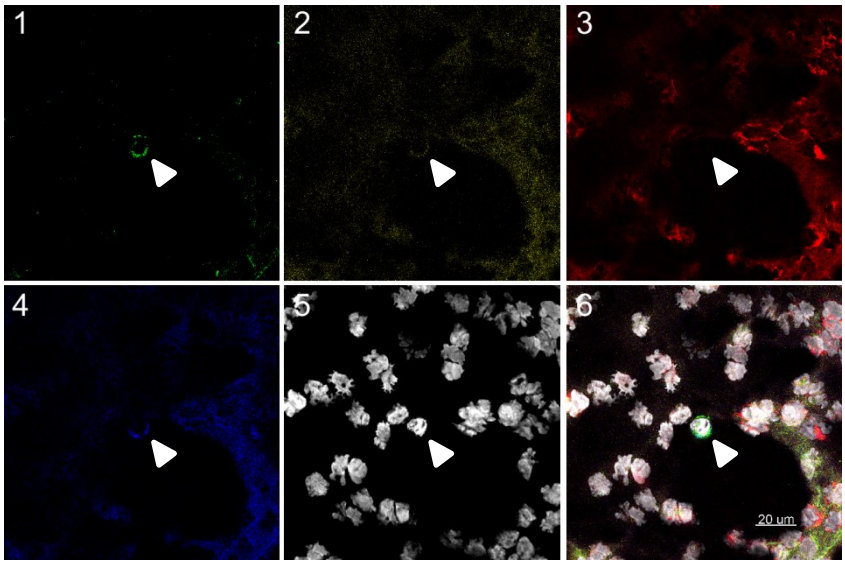

Figure 15: IF staining of patients' CTC (14095). (1) EpCAM – green, (2) HPV16 E7 – yellow, (3) CD45 – red, (4) pan Cytokeratin – blue, (5) DAPI – grey, (6) merge. Arrow indicates cervical cancer derived CTCs.

For patient 14349 the pattern of EpCAM$^+$, Cytokeratin$^+$ and HPV16 E7$^-$ remained true for three out of four detected CTCs. One single cell comprised an EpCAM$^-$, Cytokeratin$^+$ and HPV16 E7$^-$ signal (indicated by the red arrow). Among all panel 1 CTCs this single cell was the only, which is exclusively positive for a single CTC marker.

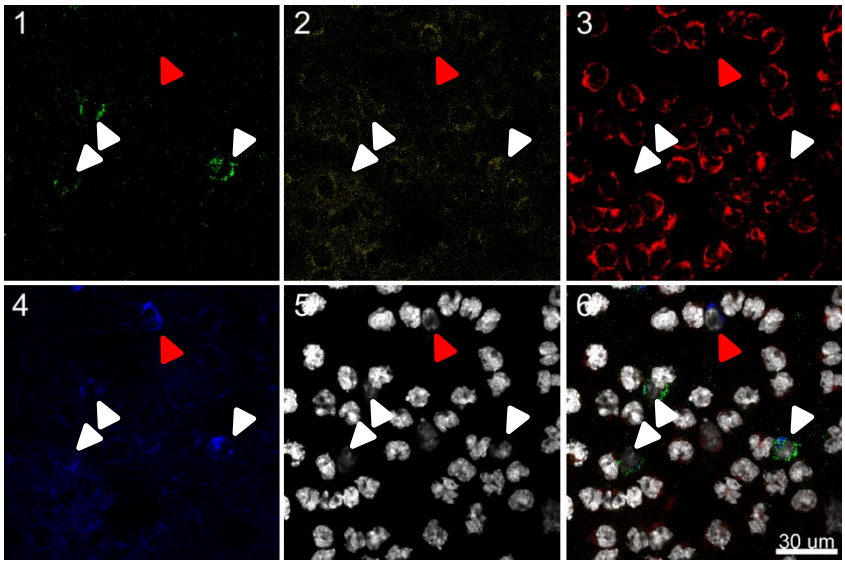

Figure 16: IF staining of patients' CTC (14349). (1) EpCAM – green, (2) HPV16 E7 – yellow, (3) CD45 – red, (4) pan Cytokeratin – blue, (5) DAPI – grey, (6) merge. Arrows indicating cervical cancer derived CTCs.

Overall, the panel 1-wise stained CTCs resulted in a consistent Cytokeratin detection. EpCAM was also detectable in nearly all CTCs, except the single cell in sample 14349. The detectability of HPV16 E7 was uneven and ranged from clearly positive to not detectable. In general the anti-HPV16 E7 antibody produced a noticeable background in all samples. Even though, the five-color immunofluorescence staining was deployed successfully and resulted in panel 1-wise delimited cervical cancer derived CTCs. The pathological FIGO staging of patients with detectable CTCs ranged from IA1 to IIB and,

if available, grades were classified as 1 and 2. An overview of the marker characteristic in all positive staining is depicted in table 6.

Table 6: Total staining results of panel 1

Patient ID	CTC quantity	CTC markers			Immune marker	FIGO	Grade
		EpCAM	HPV16 E7	Cytokeratin	CD45		
13288	3	++	++	++	-	IIB	-
13625	12	++	+	++	-	IIB	2
14095	1	+	-	+	-	IA1	1
14295	1	++	+	++	-	IB1	-
14349	4	+	-	+	-	IB2	-

(++ = very strong, + = strong , - = not detectable/unspecific)

3.3.3 Panel 2

Similar to the panel 1 approach, CTC candidates were manually identified and subsequently visualized using the CLSM. The specific wavelength setup for each fluorescent channel was adjusted according to control samples (figure 28 and figure 29) and is shown in table 3. In 6/59 (10.2%) patients CTCs could be identified.

For a CTC identification based on the high abundance of infections with high risk HPV, the second panel composition was intended to comprise an anti-HPV18 E7 specific antibody. Therefore, the anti-HPV18 E7 antibody staining was evaluated on density gradient enriched PBMCs of a healthy donor, spiked with the cervical cancer cell line ME-180. The first staining experiment (figure 17, left panel) resulted in HPV18 $E7^{+}$ and $CD45^{-}$ ME-180 cells with a general high specificity and very little background. After four weeks, a validation experiment under equal conditions exhibited a drastically reduced specificity of the antibody (figure 17, right panel). A robust, reproducible HPV18 E7 detection using ME-180 cells as positive control was repeatedly not achievable and the spiked ME-180 cells could only be identified via DAPI and $CD45^{-}$ staining. Thus, the anti-HPV18 E7 antibody-reliability was insufficient for CTC detection and it was substituted by the anti-pan-cytokeratin antibody, due to its comprehensive CTC detection in panel 1.

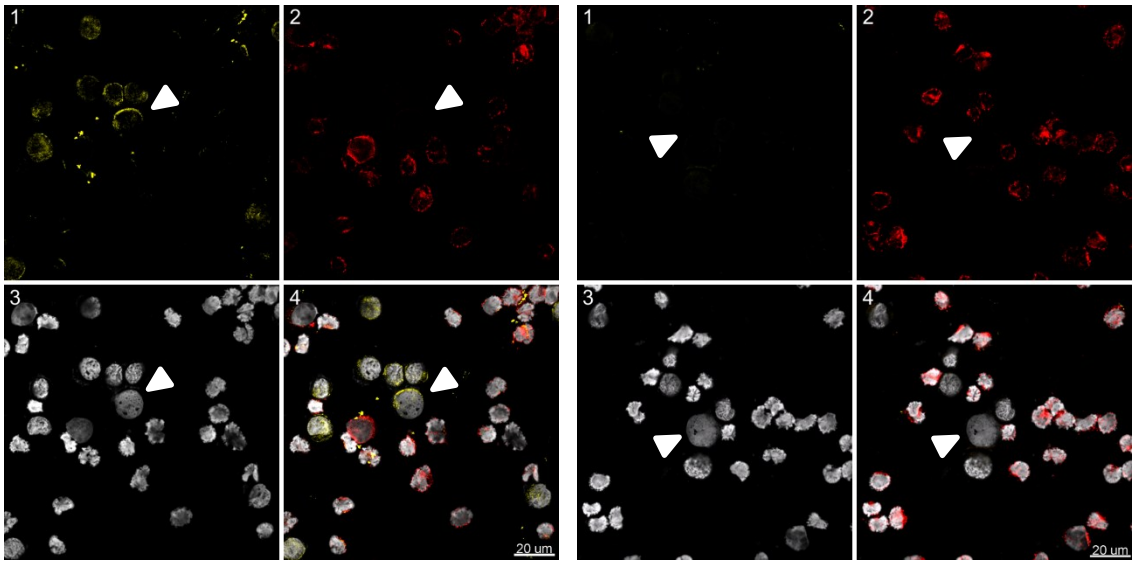

Figure 17: Evaluation of the HPV18 E7 antibody. Spiking experiments, ME-180 cells were spiked into density gradient enriched PBMCs of a healthy donor. (1) HPV18 E7 – yellow, (2) CD45 – red, (3) DAPI – grey, (4) merge. Left set: anti-HPV18 antibody specificity at time point 1. Right set: diminished specificity of the anit-HPV18 antibody within four weeks.

Sample 12571 exhibited one detectable $p16^{+}$, Cyclin $E2^{+}$, $Cytokeratin^{+}$ and $CD45^{-}$ CTC among the PBMCs (figure 18). Its fluorescence intensity, especially in the fluorescence channels for Cyclin E2 and Cytokeratin, is remarkably above the remaining cells. Although, several $CD45^{+}$ immune cells also feature a specific p16 and Cyclin E2 signal. Considering the nuclear shape of the CTC, an abnormal bulge is present in the lower nuclear section.

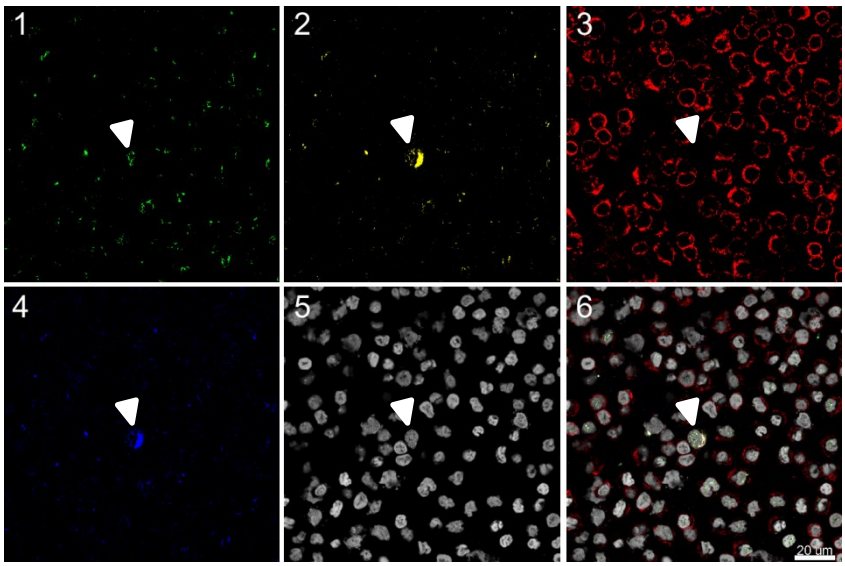

Figure 18: IF staining of patients‘ CTC (12571). (1) p16 – green, (2) Cyclin E2 – yellow, (3) CD45 – red, (4) pan Cytokeratin – blue, (5) DAPI – grey, (6) merge. Arrow indicates cervical cancer derived CTCs.

The sample of patient 13625, which comprised CTCs positive for the entire panel 1 markers, also contained two positive CTCs for panel 2 markers (figure 19 and figure 30). Detected CTCs are $p16^{+}$, Cyclin $E2^{+}$, $Cytokeratin^{+}$ and $CD45^{-}$. Although, a large number of the $CD45^{+}$ cell population features $p16^{+}$ and Cyclin $E2^{+}$ staining. This is particularly evident in figure 30, where nearly every immune cell is positive for both

surrogate markers. In addition, the Cytokeratin staining in this sample showed an uncharacteristic high level of background noise, although a discrimination of background signal, and specific signal was still possible.

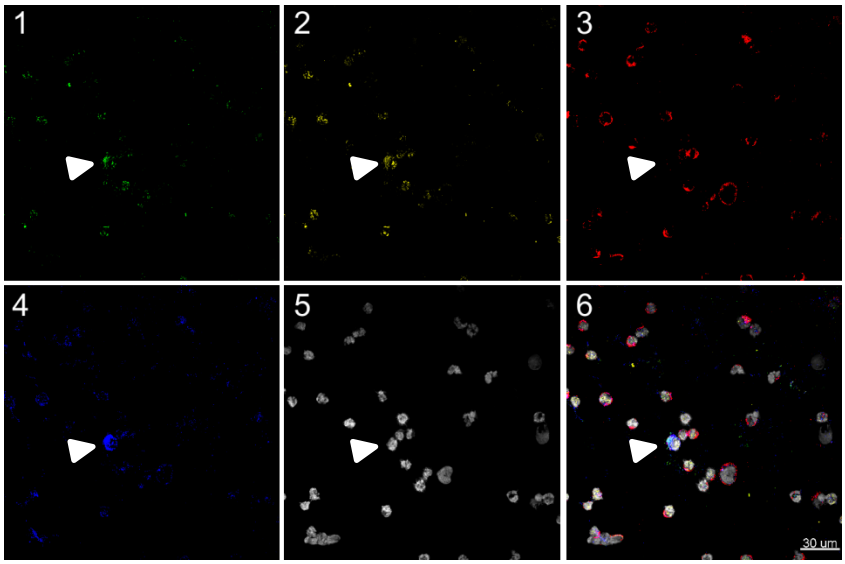

Figure 19: IF staining of patients' CTC (13625). (1) p16 – green, (2) Cyclin E2 – yellow, (3) CD45 – red, (4) pan Cytokeratin – blue, (5) DAPI – grey, (6) merge. Arrow indicates cervical cancer derived CTCs.

The pattern of positive staining results for the CTC markers and no detectable panleukocyte marker also remained true for the CTC in the sample 14670 (figure 20). Its fluorescence characteristics, however, differed slightly compared to sample 12571. For sample 14670, the Cyclin E2 staining was less strong, whereas the Cytokeratin intensity was considerably high. In addition to the weaker Cyclin E2 signal, the channel specific background was elevated, which resulted in a less delimited CTC. In this sample, the $CD45^{+}$ cells, yielding a positive p16 signal, were also of lower abundance compared to sample 12571 or 13625.

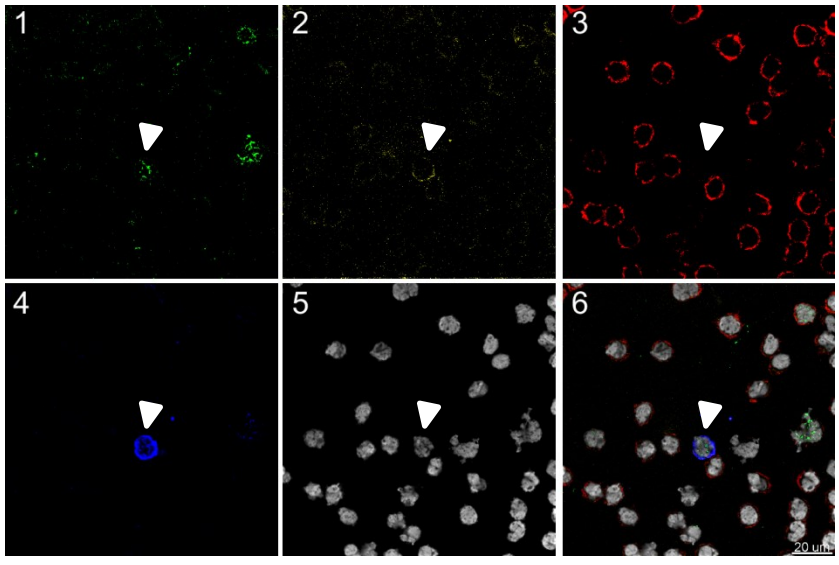

Figure 20: IF staining of patients' CTC (14670). (1) p16 – green, (2) Cyclin E2 – yellow, (3) CD45 – red, (4) pan Cytokeratin – blue, (5) DAPI – grey, (6) merge. Arrow indicates cervical cancer derived CTCs.

The staining of sample 14528 resulted in two detectable $p16^-$, Cyclin $E2^+$ and $Cytokeratin^+$ CTCs (figure 21 and figure 31). Compared to the other CTCs, the overall p16 detectability among all detected cells is of weakest occurrence. The Cyclin E2 staining produced explicit background noise.

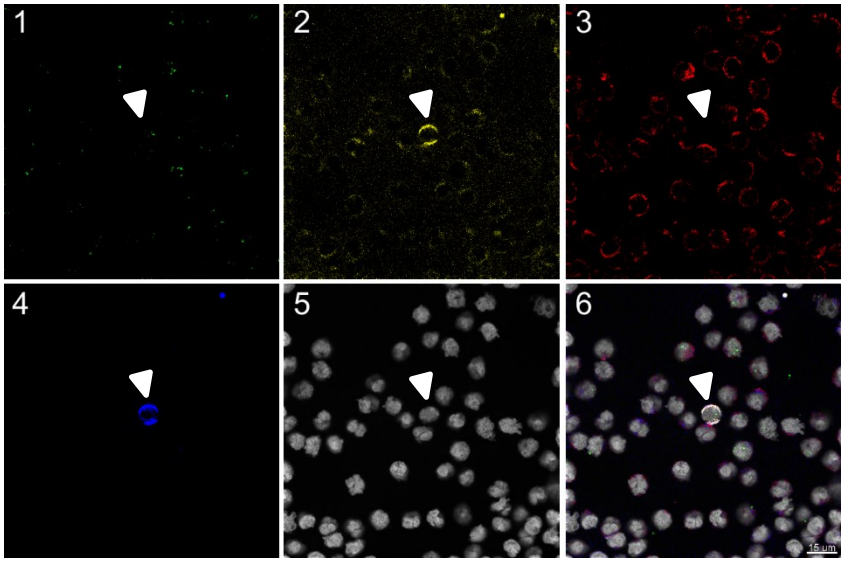

Figure 21: IF staining of patients' CTC (14528). (1) p16 – green, (2) Cyclin E2 – yellow, (3) CD45 – red, (4) pan Cytokeratin – blue, (5) DAPI – grey, (6) merge. Arrow indicates cervical cancer derived CTCs.

Both patient samples 14604 and 14697 exhibited one detectable CTC each and featured the same staining pattern (figure 22 and figure 23, respectively). Detected CTCs were $p16^-$, Cyclin $E2^-$ and $Cytokeratin^+$. In sample 14604, the p16 staining resulted in a high background in addition to several $p16^+$ PBMCs.

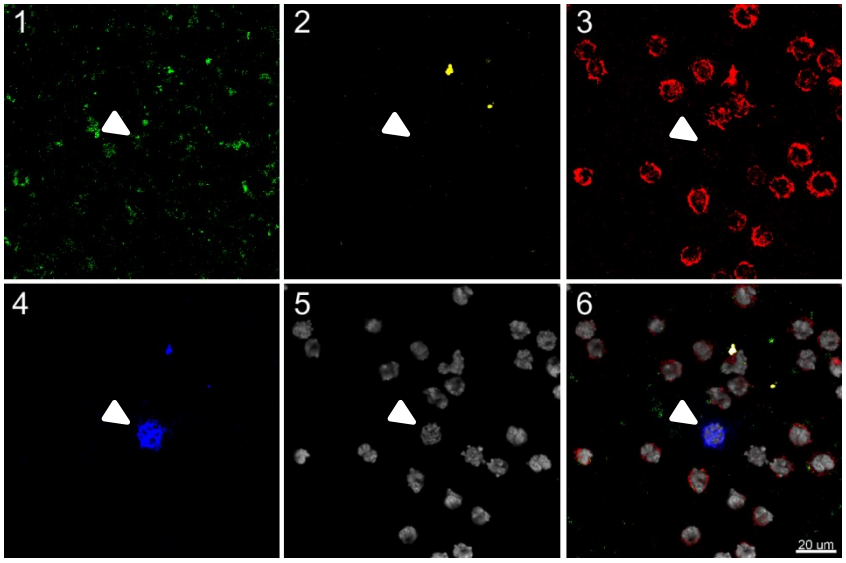

Figure 22: IF staining of patients' CTC (14604). (1) p16 – green, (2) Cyclin E2 – yellow, (3) CD45 – red, (4) pan Cytokeratin – blue, (5) DAPI – grey, (6) merge. Arrow indicates cervical cancer derived CTCs.

The rate of $p16^+$ immune cells is lower in sample 14697, nevertheless the Cyclin E2 staining produced a noticeable background. In addition to the Cytokeratin staining, the nuclear shape of the detected CTC is deformed as in sample 12571.

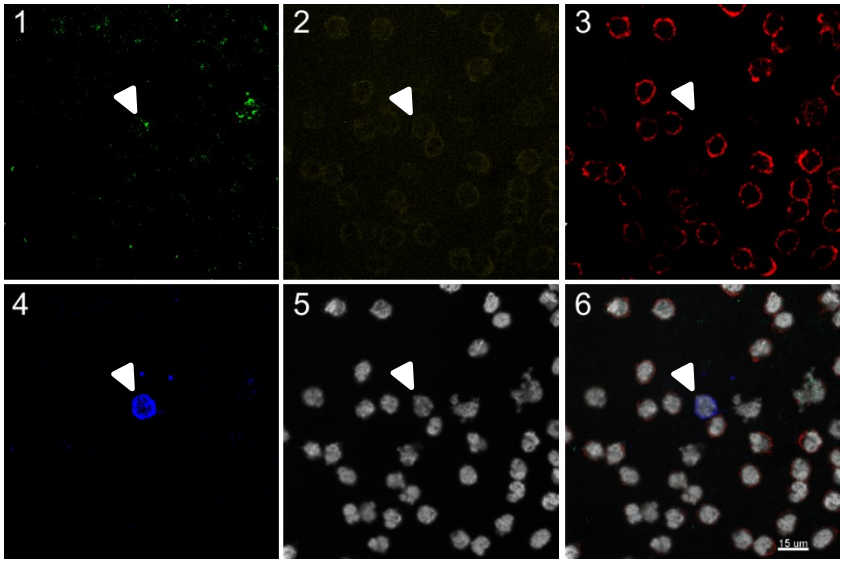

Figure 23: IF staining of patients' CTC (14697). (1) p16 – green, (2) Cyclin E2 – yellow, (3) CD45 – red, (4) pan Cytokeratin – blue, (5) DAPI – grey, (6) merge. Arrow indicates cervical cancer derived CTCs.

Taken together, the CTC staining results of the second panel are inconsistent in terms of p16 and Cyclin E2 and uniform for Cytokeratin (table 7). In certain cases, noticeable p16 staining is present in the detected CTCs, whereas others CTCs are clearly negative. Cyclin E2 staining in the CTCs is also highly ambiguous and ranged from clearly positive results to not distinguishable from the background. Furthermore, the samples 12571, 13625 and 14670 comprised a various number of $CD45^+$ cells positive for p16 and in the case of 12571 and 13625 also positive for Cyclin E2. Only Cytokeratin was consistently detectable in all samples with a high reliability. Applying the five-color immunofluorescence panel, the consistent high detectability and reliability of Cytokeratin compensated both other markers. Thus, the backing advantage of three CTC specific markers resulted in detectable CTCs using the panel 2-staining. Considering the FIGO staging, panel 2 positive CTCs were detectable in patients with FIGO IA to IIB. Grading of the same patients resulted in values between 1 and 3.

Table 7: Total staining results of panel 2

Patient ID	CTC quantity	CTC markers			Immune marker	FIGO	Grade
		p16	Cyclin E2	Cytokeratin	CD45		
12571	1	+	++	++	-	IA	1
13625	2	+	+	++	-	IIB	2
14528	2	-	+	++	-	-	1
14604	1	-	-	++	-	IB1	1
14670	1	+	+	++	-	IB1	3
14697	1	-	-	++	-	IB1	3

(++ = very strong, + = strong , - = not detectable/unspecific)

3.4 Computational image analysis

The computational image analysis for CTC detection is based on a CP pipeline, which detects and separates CTCs among PBMCs. Evaluation of TissueFAXS provided images was achieved by DAPI-based nuclear recognition and subsequent cell

definition. For each determined cell the fluorescence values of the CTC marker specific channels were identified. Using predetermined thresholds, CTCs were distinguished from immune cells by their specific fluorescence value.
The pipeline development was done using panel 1-wise stained cytospins of density gradient enriched PBMCs of a healthy donor, spiked with the cervical cancer cell line Ca Ski. The constructed CP pipeline for Ca Ski detection resulted in plausible values, without considerably false positive count. For initial CTC detection, thresholds adapted to the positive and negative controls were utilized. This strategy resulted in a remarkably high false positive quantity and low CTC sensitivity. For evaluation of the general CTC sensitivity and threshold adaption strategy, three defined, evaluated and CTC containing areas were considered. All of these areas only contain CTCs in a single FOV, fixing the true positive count to a determined value. The fluorescence thresholding values were either adapted to control or true positive CTC values. Figure 24 demonstrates the resulting CTC detection frequencies for an increasing FOV number.

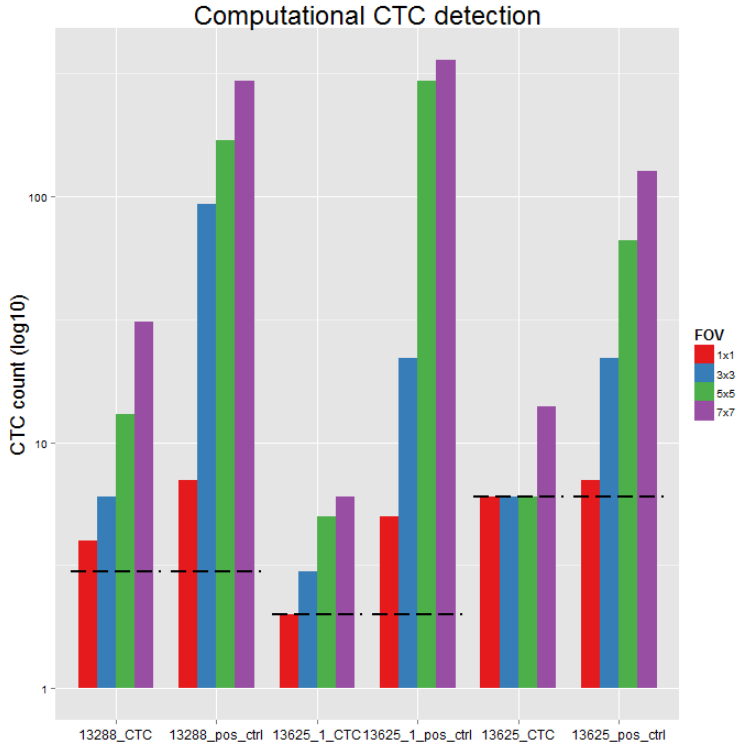

Figure 24: CellProfiler provided CTC detection (log scale). CellProfiler field-of-view-wise CTC count with CTC and positive-control-adapted thresholds. Horizontal dashed line indicates the true positive CTC value in the sample.

For sample 13288 and 13625_1 the computational CTC count increased nearly linear, whereas the control adapted thresholding strategy showed an exponential increased CTC quantity with an elevated FOV count. In sample 13625 the CTC adapted thresholding consistently detected the true positive CTC count up to 5x5 FOVs. Initially the 7x7 FOV consideration resulted in false positive CTC detection. Summarized the CTC thresholding strategy inclined towards a linear overestimation, whereas the

control adapted thresholding trended towards an exponential overestimation (see also figure 32).

A detailed overview of the obtained CP data is represented by table 8. The CTC overestimation ratio for all analyzes was calculated and consists as the quotient of the detected CTC count to the true positive CTC ratio. In general, the CTC adapted thresholding strategy results in a constantly lower overestimation rate compared to the control adapted thresholding. Although, both algorithms tended towards higher overestimation rates with increasing number of FOVs. In fact the cell count seems not to be directly related to overestimation, since a higher total cell count does not necessarily result in a higher ratio. Differences in the overestimation rate between both thresholding preferences were not significant (p-value > 0.05). However, the false positive ratio revealed a significant difference between both thresholding strategies. The experiments 13625 and 13288 exhibited significant p-values (p-value < 0.05), whereas the p-value of experiment 13625_1 was not significant (p-value >0.05).

Another peculiarity finding was a slight fluctuation in the general cell count among the experiments. Considering 13625_1 and 13288 in one of each computation a variation of one cell was detected, although the DAPI thresholds and cell recognition strategy remained similar.

Table 8: Computational analysis of TissueFAXS provided FOVs

Sample ID	Adaption strategy	FOVs	CTC - true positive count	CP – Cell count	CP – CTC count	FP ratio	CTC - overestimate rate
13288	CTC adapted	1	3	1,034	4	0.10	1.33
		9		7,642	6	0.04	2.00
		25		17,115	13	0.06	4.33
		49		37,590	31	0.07	10.33
	Pos. ctrl. adapted	1	3	1,034	7	0.39	2.33
		9		7,641	93	1.16	31.00
		25		17,115	168	0.96	56.00
		49		37,590	294	0.77	98.00
13625	CTC adapted	1	6	149	6	0	1.00
		9		1,163	6	0	1.00
		25		4,431	6	0	1.00
		49		15,323	14	0.05	2.33
	Pos. ctrl. adapted	1	6	149	7	0.69	1.17
		9		1,163	22	1.36	3.67
		25		4,431	66	1.33	11.00
		49		15,323	126	0.78	21.00

13625_1	CTC adapted	1	2	1,064	2	0	1.00
		9		7,764	3	0.01	1.50
		25		21,430	5	0.01	2.50
		49		40,456	6	0.01	3.00
	Pos. ctrl. adapted	1	2	1,065	5	0.28	2.50
		9		7,664	22	0.26	11.00
		25		21,430	294	1.34	147.00
		49		40,457	358	0.87	179.00

3.5 HPV genotyping

For HPV genotyping paired Pap-smear and FFPE biopsy samples of CIN patients were analyzed using PapilloCheck®. Pap-smear samples were treated according to the PapilloCheck® protocol. FFPE samples were preprocessed, for which various sections were deparaffinized. Extracted tissue samples were further processed according to the protocol (see chapter 2.2.3).

The utilized cellular amount of the Pap-smear samples was not quantifiable, since the samples were stored at -20 °C. Additionally a general erythrocyte contamination was present in all samples. The quality and tissue quantity of provided FFPE samples was highly diverse. In particular, the tissue area ranged from approximately > 1 mm^2 to nearly 1 cm^2. In two cases the amount of epithelial tissue was insufficient and the general quality was below average. Both samples were expelled from further analysis. As processing controls aliquots of SiHa cells were treated either according to the Pap-smear or FFPE protocol (see chapter 2.2.3).

The fluorescence-readout was performed by an external cooperation partner. It was achieved by using an excitation wavelength of 635 nm for the sample and PCR control, whereas the hybridization and genotyping results were assessed by 532 nm excitation. The resulting fluorescence values were detonated as signal to noise ratios (SNR), whereas positive thresholds were determined as SNR-values above 20.

In first experimental transition 3x5 µm FFPE sections were deparaffinized using 1,000 µl xylene. All other experimental parameters were conducted according to the protocol. The detected fluorescence values are depicted in table 9. In all samples the PCR control values were above the threshold, therefore a general PCR amplification of genetic material was accomplished. Among all Pap-smear samples, the experimental SNRs were above the confidence threshold. Furthermore, obtained Pap-smear genotypes corresponded to the previously known HPV subtypes. Altogether the Pap-smear genotyping results were very consistent and trustworthy. In opposite, the FFPE genotyping results were highly ambiguous. Only the FFPE sample 10748 showed comparable SNR values when compared to the Pap-smear results. The three FFPE samples 10981, 10647 and 11012 were lacking detectable genotyping signals, but held reliable sample and PCR control values. In the case of 11152 and the SiHa FFPE-

extraction-control, weak HPV genotyping and strong PCR control signals were detected. Although, interestingly no sample control signal was verifiable.

Table 9: PapilloCheck® genotyping results - first experimental round

Sample type	Sample ID	CIN	HPV Genotype	HPV-SNR	Sample control	PCR control
Pap-smear	10748		HPV16	6,569.2	5,424.1	301.3
	10981		HPV16	4,907.7	5,359.4	410.6
	11152		HPV31	3,633.1	5,666.2	981.8
	10647		HPV16	5,058.7	5,511.2	298.0
			HPV53	227.1		
			HPV59	76.0		
	11012		HPV42	3,835.1	5,504.9	1,484.4
	SiHa		HPV16	4,357.2	6,069.8	2,315.6
FFPE	10748	2	HPV16	4,847.1	879.0	3,094.0
	10981	3	-	-	1,420.2	3,036.3
	11152	1	HPV31	20.7	-	3,097.2
	10647	3	-	-	839.6	3,091.1
	11012	2	-	-	3,021.8	3,254.3
	SiHa		HPV16	162.5	-	3,088.1

In the second HPV genotyping experiment a revision of Pap-smear samples was spared. However, the experimental parameters were slightly adapted and samples were processed in duplicates. In that course 5x5 µm FFPE sections were deparaffinized using 500 µl xylene. All remaining experimental parameters were conducted according to the protocol. The detected fluorescence values are shown in table 10. In general, the overall high PCR control values indicated a successful PCR amplification. Although the genotyping results were highly divers, even the results of the individual replicates varied. As only exemption, the sample 10748 results were consistent and corresponded to the previous experiment. Both samples 10981 and 11012 remained negative in genotyping and only one sample control resulted in a reliable SNR value. The genotyping results of the samples 11152 and 10647 were considerably ambiguous. Only one duplicate of each sample yielded a positive genotyping, whereas the respective other one did not verify this result. Furthermore, the sample controls of these specimens were consistently negative. Results of the SiHa FFPE-extraction-control exhibited strong SNRs among all readout parameters, indicating a principal extraction and PCR amplification success for FFPE samples.

Table 10: PapilloCheck® genotyping results - second experimental round

Sample type	Sample ID	CIN	HPV Genotype	HPV-SNR	Sample control	PCR control
FFPE	10748	2	HPV16	4,959.3	435.1	3,229.8
				4,830.2	411.8	3,047.6
	10981	3	negative	-	-	3,736.5
				-	403.9	3,997.1
	11152	1	HPV16	344.9	-	4,014.3
			negative	-	-	4,279.7
	10647	3	HPV16	66.8	-	4,605.1
			negative	-	-	4,014.3
	11012	2	negative	-	-	3,866.5
				-	-	4,101.1
	SiHa		HPV16	4,300.7	5,210.5	3,342.9
				3,548.9	4,660.0	2,913.2

Summarized, Pap-smear genotyping resulted in reliable and reproducible HPV genotyping, which entirely matched to previous results. However, the FFPE based genotyping did not reveal any general reproducibility or reliability. Therefore, a possible correlation between the cervical neoplasia grade and the capability of genotyping could not be established. The amount of utilized FFPE tissue material seems also not to affect genotyping results. In fact, the only clinical sample with consistent and plausible results (sample 10748) had one of the lowest overall tissue content.

4 Discussion

Circulating tumor cells in the peripheral blood are the main factor for metastatic spread to distant organs [114]. In cervical cancer patients, the detection of CTCs may represent a way of metastatic spread assessment, prediction of relapse and in case of clinically treated patients, an opportunity for monitoring and relapse diagnosis. This is of major interest, since there is an especially high need for methods, allowing a reliable, specific and non-invasive relapse monitoring. Although clinical therapy comprises chemotherapy, radiation therapy or surgery, a complete elimination of all tumor content may not be achieved in all cases and especially micrometastases in distant organs, lymph nodes or the bone marrow may survive the clinical treatment. The recurrence rate varies with stage and has been reported to be between 10-20% in patients with stage IB-IIA and no involvement of lymph nodes [115, 116]. However, women with locally advanced tumors and/or nodal metastases will relapse in up to 70% of cases [117, 118]. For these patients, a blood based monitoring of the presence of CTCs may constitute an additional way for relapse monitoring, well before current imaging techniques are capable to detect recurring metastatic tumor growth [89]. Furthermore, the usage of liquid biopsies for CTC screening represents a noninvasive and a patient-friendly diagnostic method. For the detection of CTCs, immunofluorescence staining based technologies have been shown to be valuable, but in case of cervical cancer, no such method is established, yet [89]. Therefore, the linkage of a reliable and cervical cancer specific five-color immunofluorescence staining with a computer based image evaluation could enable an additional and high throughput based method of clinical application.

4.1 TissueFAXS

The TissueFAXS image acquisition was intended to provide the image-basis for the computational and manual CTC identification. The obtained cytospins varied in their overall staining quality, when visualized by the TissueFAXS. One conspicuous attribute was an enormous background fluorescence of many samples in the 488 nm wavelength channel among both panels (figure 11). In contrast, neither the staining control samples nor the slides for panel development exhibited this feature. Since this background was panel-independent and all samples were treated equally, one could only speculate that in some cases the density gradient centrifugation may strained the cells and time differences in cytospin preparation facilitated cellular lysis. Hence, the blocking might have been insufficient and could facilitate an unspecific secondary antibody binding. In some cases overlapping segments caused areas with an excessive fluorescence level, which also resulted in overlapping fluorescence signals and crosstalk. It seems that the surface detachment is related to the cell density, since it frequently occurs in areas of large cell number. Thus, a standardized cell count might solve this issue, although the exact reason remains unclear. A further fluorescence

related issue of the TissueFAXS evaluation, results from the control adapted exposure times of each marker specific channel. Since the control adapted exposure timing was adjusted to the uniform control staining, the heterogeneity and general diversity of the patient samples may have contributed to the background noise. Additionally the expression of all CTC specific markers was consistent and in general, at high-level in the utilized cell lines. Thus, the exposure time for the CTC marker channels was relatively short. From this follows that, the exposure time might be insufficient to capture CTCs with declined marker expression values. A decrease in the expression level of certain markers could for example be the case, when cells undergo EMT. This might lead to a reduced signal of epithelial markers as for example EpCAM. A further circumstance is the slight focus shift in certain FOVs, caused by the utilized focus strategy. This drawback is a tradeoff between focal accuracy and scan time. Although a focus adaption for every FOV is feasible, the acquisition time would increase substantially. TissueFAXS image acquisition, however, is an appropriate method to scan the processed cytospins. The majority of obtained images are of good quality and adequate for downstream processing. Although a major improvement of obtained images could mainly be attained by an adaptation of the cytospin preparation protocol. On the on hand, an alternative CTC enrichment method, utilizing different CTC characteristics like plasticity and enlarged size, might minimize cellular stress and does not result in lysis. On the other hand, a standardized cell number might prevent for overlapping segments.

4.2 CTC marker specific immunofluorescence

After extensive testing on different cell lines and PBMC fractions of whole blood as negative controls, the appropriate dilutions and the general antibody specificity could be confirmed as adequate for both panel specifications.

It was chosen to apply a five-color immunofluorescence based detection. This means, that additionally to the nuclear staining, four different targets can be tested at once. The establishment of such a staining approach is labor-intensive, but has many advantages. On the one hand CTCs are very rare cells and have to be detected in a high background of immune cells present in the blood. Thus, the five-color immunofluorescence detection has the advantage of a specific indication based on the presence of three CTC makers. This threefold indication serves on the one hand as an increase of specificity, but, on the other hand, facilitates the detection, even though not all markers are convincingly. The more markers can be observed in parallel, the more information can be gained at once. Otherwise it would be necessary to process a higher blood volume to obtain the same information, which is often not feasible. Furthermore, it was shown that CTCs are heterogeneous within one entity, and partially even within one patient. They can also undergo processes like EMT and change their properties. For those reasons a detection based on only one marker would lead to reduced sensitivity. Also, this method is flexible and if literature comes up with new markers suitable for

CTC detection, the panel of antibodies can be altered. An additional advantage of this method is that it allows a quantification of CTCs, which according to different literature could be of prognostic value [119-121].

The combined application of the five-color immunofluorescence panels was subsequently implemented and resulted in a reliable detectability of the utilized cervical cancer cell lines. Hence, the identification of cervical cancer cell lines was possible by merging the CTC marker and DAPI specific signals. The retained PBMCs were detectable due to CD45 and DAPI staining.

On the basis of the established cervical cancer CTC markers, a general detection of tumor derived CTCs was achieved in 10/59 (16.9%) patients with cervical cancer at time point of primary diagnosis. The staining of patient samples using panel 1 antibodies resulted in 5/59 (8.5%) samples with detectable CTCs, differing in their overall marker characteristics (table 6). All detected CTCs resulted in a positive Cytokeratin staining. EpCAM was also present in all CTCs, except a single cell in sample 14349. HPV16 E7 was present in three out of the five samples and also resulted in notable staining varieties. A detection of CTCs varying in HPV16 E7 marker intensity was expected, especially since the genotypes of the examined samples were not known. Therefore, the detection of $EpCAM^{+}$, $Cytokeratin^{+}$ and HPV $E7^{-}$ cells is plausible. However, in the two samples lacking a specific HPV16 E7 signal the general background level is elevated, which also results in lesser specificity for EpCAM and Cytokeratin. Thus, a lower overall specificity and cross reactions may have resulted in a HPV16 E7 masking and no distinguishable fluorescence values. Considering the $EPCAM^{-}$, $Cytokeratin^{+}$ and HPV16 $E7^{-}$ CTC in sample 14349, a final clarification why it is exclusively Cytokeratin positive, is not possible. One possible explanation could be an undergoing EMT. In this particular case, the expression of the epithelial protein EpCAM might by decreased, resulting in staining intensity at background level. In this case, however, a simultaneous down regulation of the Cytokeratin expression would be conceivable. The general FIGO stage of the patients with identified panel 1-wise CTCs ranges from IA1 to IIB. Other than initially expected, CTCs were detectable in patients with comparatively lower FIGO staging. In three out of five cases the tumor is confined to the cervix; in the two remaining cases, the carcinoma extended beyond the cervix. Grades were available in two out of five patients and ranged from 1 to 2. However, the number of five patients with detected CTCs did not permit further statistical correlation analysis with FIGO stage or grade.

To include the second most abundant HPV genotype in the marker panel, an anti-HPV18 E7 antibody was evaluated in dilution experiments. Repeated experiments under corresponding conditions revealed a drastically diminishing specificity. Since the usage and storage were conducted according to the manufacturer's specifications, the decreasing specificity could not be assigned to a particular reason. Although, the antibody is not yet commercially available, this issue might be eliminated in the final product.

The 6/59 (10.2%) CTC-containing samples of panel 2 exhibited diverging p16 and Cyclin E2 detectability, whereas Cytokeratin was constantly strong and reliable (table 7). Comparing the Cytokeratin detection to the first panel, the second panel characteristic remained constantly high and at an equal level. Both cervical cancer surrogate markers were also detectable, despite not all Cytokeratin$^+$ CTCs exhibited staining for either marker. During the image evaluation a general issue in the usage of p16 and Cyclin E2 emerged. The patients 12571 and 13625 exhibited specific staining for p16 and Cyclin E2 among the CD45$^+$ PBMC population (figure 18 and figure 19). Since both proteins are involved in the cell cycle, activated PBMCs may also express either marker. Although a certain elevation was expected, the detected quantity of activated immune cells was tremendous in both samples. Thus, both p16 and Cyclin E2 are indeed detectable in cervical cancer derived CTCs, but comparable detectability in CD45$^+$ cells impairs their validity and cervical cancer specificity. Further interesting aspects are the uniformly low FIGO stages. Likewise panel 1 result, relatively low FIGO stages of samples positive for panel 2 markers, between IA and IIB, were unexpected. Grading in the CTC positive samples ranged from 1 to 3. A correlation of CTC results to FIGO stages or Grade was also not viable for the second panel.

In combined consideration only the patient 13625 exhibited CTCs positive for all makers among both panels. All remaining samples were either positive for one or the other marker panel. Considering the detected CTC count of patient 13625, the comparably high number, especially detectable in panel 1, might be the reason for detectable CTCs in both panels. In contrast, the small number of CTCs identified in the remaining patients, might be the logical explanation for positive results in only one of the applied panels.

In overall consideration the initially stated hypothesis could be verified. The examination of all obtained staining results showed the applicability of the five-color immunofluorescence staining. In cases of multiple CTC marker detection, CTCs could be detected and identified. Although, cases like 14528 and 14697, where only one marker was detectable, also demonstrated the benefit emerging form the fivefold staining. In both cases the presence of a reliable Cytokeratin staining ensured the classification as CTCs and the absence of, up to two, cervical cancer specific markers was compensated. Furthermore, an advantage of either five-color immunofluorescence panel is a simple adaptability. Primary antibodies are substitutable without additional adaptations, as long as their species and isotype correspond. Thus, an extension of the marker panel is easily accessible. For this reason, the five-color immunofluorescence panel is a reasonable approach for CTC detection. Furthermore, the detection of cervical cancer derived CTCs utilizing the hypothetical markers could be achieved. For that the epithelial markers Cytokeratin and EpCAM are well established and most reliable. CTC detection via the essential HPV derived protein E7 was also possible via the novel anti-HPV16 E7 antibody. However, this marker does not add additional information to the established epithelial markers, but an application is suitable. HPV-surrogate markers, Cyclin E2 and p16, are not capable to indicate HPV derived CTCs on their own.

Although several CTCs were positive for at least one marker, the indication of proteins involved in the cell cycle was too unspecific, especially among possibly proliferating PBMCs. The validity of every tested cervical cancer specific marker for the IF based detection of CTCs is depicted in table 11.

Table 11: Validity of the tested cervical cancer markers for IF based CTC detection

Marker	Validity
Cytokeratin	++
EpCAM	+
HPV16 E7	o
Cyclin E2	-
p16	-

(++ = very valid, + = valid, o = suitable, - = inappropriate)

All obtained staining results are based on a single experimental run using each panel. For more convincing statements and a general higher reproducibility the number of cytospins per patient should be increased. This might also lead to more panel-overlapping positive result and possibly enables more statistical analysis. Unfortunately, a higher number of cytospins for parallel analysis is difficult to achieve and was therefore also not performed in this study. It would require larger blood volumes (4.5 ml / cytospin), which is often not feasible.
Furthermore, the consideration of prospective clinical follow-up data will be of highest interest. At time of writing, relapse information of only a limited number of patients was available. However, at a later stage, the correlation of relapse information to the presence of CTCs at primary diagnosis might assess CTCs as prognosis factor in cervical cancer. A general coherence of CTCs at primary diagnosis was shown in other cancer entities, like breast, prostate and lung cancer, and generally correlates with a poor prognosis [119-121]. Thus, a comparable effect in cervical cancer is conceivable and might be indicated by the overall survival. Furthermore, progression-free survival might also indicate a correlation between CTC-detectability at primary diagnosis and clinical recurrence. In addition, the consideration of metastases formation in CTC-positive patients compared to CTC negative patients may be evaluated, possibly resulting in an earlier metastases formation in positive patients. Overall, these considerations might facilitate an estimation of cervical cancer CTCs as a possible prognostic factor and consider their deployment in relapse diagnosis.

4.3 Computational image analysis

For image analysis, the CP pipeline was developed and optimized based on staining control samples. The initial control adapted strategy resulted in a non-evaluable high amount of CTC candidates, including a remarkable false positive quantity and overestimation rate (table 8). Both issues became especially apparent with an increasing

number of FOVs, where the overestimation rates increased to values between 18-fold to 71-fold. The thresholding adaption to the precise fluorescence values of the identified CTCs radically alleviated both, the false positive count and the overestimation rate. Thus, the overestimation declined to a 2-fold and 10-fold overrating. Considering both different threshold adaptations, the control adaption trends towards an exponential overestimation, whereas the CTC adaptation inclines towards a linear overestimation (figure 24 and figure 32). One reason for the higher overestimation of the control adapted CTC identification is the setup of the thresholding strategy. Since, thresholds are calculated based on the distribution of the mean intensities, low intense background staining and artifacts of high intensity are widening the distribution. Based on this extended range, PBMCs, featuring certain background staining or artifacts in close proximity, are incorrectly identified as CTCs. In contrast, the sharper defined CTC adapted thresholds do not cover this type of deviations. However, a certain level of false positive CTCs still remains in the CTC adapted thresholding. Although, a significant reduction of the false positive ratio (p-value < 0.05), considering both adaption strategies, could be shown in two-thirds of the experiments. A further problem for the automated image based CTC detection was the TissueFAXS exposure setup. Since the exposure times were adjusted to cell lines, which are supposed to highly express certain antigens, only CTCs with a comparable expression level are acquired with sufficient precision. Thus, CTCs with antigen expression rates below certain values cannot be recognized by the CP pipeline. Furthermore, the cell-independent cytospin preparation resulted in a very heterogenic cell density and during processing, areas overlapped (figure 11). This irregular pattern had a noticeably influence on the automated assessment. For example, the staining intensity of overlapping areas deviated in magnitudes compared to single cells. Thus, the high intensity values principally resulted in exclusion and non-evaluable areas, since DAPI provided nuclear recognition is impaired and neither thresholding strategy covered the corresponding values.

A possible approach to improve and further develop the CP pipeline would be the deployment of machine learning techniques and the addition of broader characteristics, in addition to the fluorescence intensity. Initially a machine learning algorithm would be practiced based on true positive CTCs. This would lead to a recognition model, built up by the inputs and results in a CTC adaption model, which considers more detailed parameters like background fluorescence, artifacts and general illumination. Furthermore, the integration of morphological characteristics like the nuclear shape and distinct staining characteristics might further diminish the false positive CTC recognition rate. Especially, artifacts within the CP defined cytoplasm were considerable and could possibly be diminished with an adaptive machine learning approach.

4.4 HPV genotyping

This proof of principle was intended to clarify a possible follow-up investigation, in which cervical cancer derived CTCs could possibly be detected via a HPV dependent

gene expression-based method. With this method, the immunofluorescence-wise considered patient samples could be screened for cervical cancer derived CTCs, based on the HPV associated oncogenic gene expression, via a quantitative PCR approach on nucleic acid level. For the establishment and evaluation of such a method, the specific HPV genotype of each patient and sample is mandatory. But since clinical routine treatment does not necessarily comprise detailed HVP genotyping, only a limited number of known genotypes were available for such an establishment. Therefore, this subproject aimed to clarify the possibility to achieve HPV genotyping on the basis of available pathological FFPE biopsies. For this, a commercially available test for HPV genotyping, which is routinely used for the analysis of Pap-smear samples, should be tested concerning its applicability for FFPE tumor tissue. As basis for this elaboration, paired Pap-smear and biopsy samples of CIN patients were assessed.

In the last decades several different HPV genotyping methods have been developed, focusing on clinical usage. These systems are mainly designed for cervical Pap-smear samples and focus on the rapid and reliable detection of the most clinical abundant HPV subtypes. More recent, complex systems like PapilloCheck® were developed, allowing the screening of a broader genotyping range linked with a higher throughput. However, the genotyping methods are basically designed for routine analyses, rather than clinical research based on FFPE biopsies. For FFPE genotyping primer systems, targeting different viral proteins, have been tested and resulted in an overall poor genotyping performance [109]. On the one hand, this is due to DNA denaturation and fragmentation during fixation. On the other, the formalin mediated cross-linking activity leads to non-reproducible molecular aberrations, which might influence the manner of common polymerases [110]. Hence, a reliable genotyping method based on FFPE may facilitate and extend the research possibilities in the field of cervical cancer.

In the first genotyping experiment (table 9), the PapilloCheck® mediated HPV genotyping using Pap-smear samples resulted in overall high SNR ratios and, compared to the previously known genotypes, in general consensus. Thus, PapilloCheck® has the capability to reproduce credible genotyping results even after a long period of sample storage, considering Pap-smear samples. In the case of FFPE material, the genotyping results are very inconsistent and do not follow a specific pattern. The high PCR control SNRs indicate a positive PCR amplification of the artificial plasmid and point towards viable amplification. Sample 10748 exhibited SNR values comparable to its corresponding Pap-smear sample and because of that, this single genotyping can be seen as plausible. Three samples did not exhibit a positive HPV genotyping, although all samples were pathologically classified as CIN. Interestingly, all of these samples are rated as advanced stages with distinct neoplasia. Although, all of these samples exhibited a distinct sample control SNR, indicating the presence and amplification of intact ADAT. One patient sample and the SiHa control exhibited no sample control, but, however, a genotyping result corresponding to the respective Pap-smear sample. This

pattern might occur in the case of very little starting material. Thereby, the low genomic amount and the general FFPE based fragmentation may lead towards a partial amplification of ADAT1 or the polymerase may favor the HPV locus. To avoid low FFPE material usage, the sample amount for the second genotyping experiment was increased. Simultaneously, the amount of xylene during deparaffinization was reduced, to prevent a possible discard during processing.

In the second genotyping experiment (table 10), the considerably inconsistent pattern remained true for most of the samples. All PCR sample controls were in a reliable range, indicating the successful amplification of the artificial plasmid. However, sample 10748 verified its previously plausible results and the SiHa extraction also resulted in plausible SNR values. In turn, the four remaining samples did not result in trustable genotyping results, since both duplicates exhibited diverging results. In the case of sample 11152, the identified genotype (HPV16) differs compared to the previous FFPE sample and the corresponding Pap-smear (both HPV31). Since the sample control is negative in this particular case, it is difficult to interpret this variance. This samples is classified as CIN I, which corresponds to an early neoplasia stage. Because of the fact that the Pap-smear sample and the corresponding biopsy are not taken at the same time point, a coinfection after the Pap-smear sampling is possible in early CIN grade. Therefore, both results could possibly be true, but a final clarification is not possible.

Taken together, a FFPE based HPV genotyping using PapilloCheck® could not be established. Only the SiHa control and the FFPE sample 10748 resulted in reproducible and plausible results. All other FFPE samples yielded variable results. In general, different sampling time points of Pap-smear samples and biopsies are problematic. With an increasing time span between both events, the probability of clinically relevant changes is increased. This is especially true in lower CIN grades, which may decay in a lower period of time, and for coinfection, which can change in composition and shift towards advantaged genotypes. A further problem is the not quantified usage of genomic material utilized in the PapilloCheck® system. The high cell count in Pap-smear samples and relatively efficient DNA extraction are leading to a general high DNA concentration, which resulted in valid genotyping results in the first run. In case of the FFPE material, the cell amount is highly divers and vigorously fluctuates among different samples. The amount of starting material, however, seems not to affect the genotyping outcome. An increased amount of FFPE starting material had no considerable effect in the second genotyping experiment. In addition, only sample 10748 showed plausible genotyping results, albeit it had the lowest amount of tissue material in this study. More important in the case of FFPE samples, the DNA extraction is more difficult. Thus, an adaptation of the lysis and elution-procedure for the FFPE material might result in a higher DNA yield. Compared to FFPE-dedicated DNA extraction protocols, the cell lysis is 8 times shorter in the utilized protocol. Therefore, an extended lysis might result in a higher amount of elutable DNA. The elution-volume could be additionally decreased to elevate the obtained DNA concentration.

5 Conclusion

The general viability of the marker panel for an antigen based immunofluorescence detection of cervical cancer derived CTCs via manual and computational image analysis could be shown in this study. The tested markers in combination with immunofluorescence detection are an adequate method to identify cervical cancer derived circulating tumor cells within the pre-enriched fraction of PBMCs. The established five-color immunofluorescence panels provide the possibility to detect multiple antigens in a single step and facilitate a detailed CTC identification. For this approach the general and widely used epithelial markers Cytokeratin and EpCAM achieved the most reliable results. In addition, HPV16 E7 integration is feasible, but does not result in further specificity. Both HPV-surrogate markers, Cyclin E2 and p16, are too unspecific for CTC detection, since PBMCs might yield comparable staining results.

To my knowledge, this is the first study, which demonstrates the successful establishment of an immunofluorescence staining procedure in the area of cervical cancer CTC research by utilizing the parallel application of five specific markers. Therefore, the limited availability of primary literature made it necessary to establish both the markers and the five-color immunofluorescence staining from the ground up. Thus, this study forms the basis on which further studies, focusing on immunofluorescence-based cervical cancer CTC detection, might build on.

The immunofluorescence based detection of CTC-specific antigens is an adequate method to identify the low quantity of CTCs within the blood. With the generation of the cervical cancer marker panel and the computational image analysis, the foundations for an additional method of cervical cancer relapse monitoring could possibly be laid. Such a post-therapeutic screening could be able to indicate a recurring cancerous growth based on the presence of CTCs in the peripheral blood. Although, to achieve this objective, further research for cervical cancer specific markers and, especially, further development of the image analysis have to be done. Therefore the five-color immunofluorescence panel offers the advantage of simple adaptability. All tested markers are substitutable, as long as the species and isotype of the antibodies correspond. Thus, substitution of a marker can be achieved easily. Since HPV derived proteins are a reasonable evidence of the CTC origin, the application of a genotype unspecific anti-HPV E7 antibody could result in an additional layer of information. This is especially critical in EMT undergoing cells, lacking utilizable epithelial markers. Nevertheless, genotype specific HPV E7 antibodies are relatively new to the market and since HPV E7 is highly variable, the development of a genotype unspecific antibody might take additional time. With a further developed and more sophisticated image analysis the false positive rate could possibly be decreased, leading to a more reliable recognized CTC count. In addition to the imaging based methods and for the elaboration of a gene

expression-based CTC detection further HPV genotyping methods have to be examined.

One restriction of the study was the small amount of patient material. This resulted in an experimental limitation of a unique panel-wise staining for each patient. An increased availability and subsequently the integration of biological replicates would definitively increase the overall validity. Furthermore, an enlarged patient cohort could further enhance the overall validity.

For an outlook on the further course of cervical cancer relapse monitoring, the evaluated markers and the five-color immunofluorescence staining have to be tested in a patient cohort with distant metastases. For that, a sufficient number of patients have to be evaluated over a prolonged period of time. In this setting, the CTC based method has to be compared to the already deployed monitoring strategies. Thereby an application of the immunofluorescence based CTC detection is only conceivable, if this method provides a significant improvement in the overall detectability.

6 List of Abbreviations

ADAT1	Adenosine deaminase, tRNA-specific 1
APC	Antigen presenting cell
BSA	Bovine serum albumin
CD45	Receptor-type tyrosine-protein phosphatase C
Cdk2	Cyclin-dependent kinase 2
CIN	Cervical intraepithelial neoplasia
CK	Cytokeratin - Keratin
CLSM	Confocal Laser Scanning Microscope
CP	CellProfiler
CTC	Circulating tumor cell
Cyclin E2	G1/S-specific cyclin-E2
E2F	Transcription factor E2F
E6-AP	E6-associated protein
EGF	Epidermal Growth Factor
EMT	Epithelial-mesenchymal transition
EpCAM (CD326)	Epithelial cell adhesion molecule
FCS	Fetal calf serum
FFPE	Formalin fixed paraffin embedded
FIGO	International Federation of Obstetricians and Gynaecologists
FOV	Field of view
HAT	Histone acetyltransferase
HDAC	Histone deacetylase
HPV	Human papillomavirus
hTERT	Human telomerase reverse transcriptase
IFN	Interferon
IFNAR	Interferon-α/β receptor
IRF3	Interferon regulatory factor 3
ISG	Interferon-stimulated gene
ISGF3	Interferon-stimulated gene factor 3
ISRE	Interferon stimulated response element
MHC	Major Histocompatibility Complex
ORI	Origin of Replication
p16	Cyclin-dependent kinase inhibitor 2A
p21	Cyclin-dependent kinase inhibitor 1
PBMC	Peripheral blood mononuclear cell
PBS	Phosphate buffered saline
pRB	Retinoblastoma protein
SNR	Signal to noise ratio

7 References

1. Stewart, B.W. and C.P. Wild, *World cancer report 2014*. 2014, Lyon: IARC Press. ixv, 630 p.
2. Bray, F., et al., *GLOBOCAN 2000 : Cancer incidence, mortality and prevalence worldwide*. 2001, International Agency for Research on Cancer: Lyon. p. 1 CD-ROM.
3. Guan, P., et al., *Human papillomavirus types in 115,789 HPV-positive women: a meta-analysis from cervical infection to cancer.* Int J Cancer, 2012. **131**(10): p. 2349-59.
4. Bernard, H.U., et al., *Classification of papillomaviruses (PVs) based on 189 PV types and proposal of taxonomic amendments.* Virology, 2010. **401**(1): p. 70-9.
5. Fidler, I.J., *The pathogenesis of cancer metastasis: the 'seed and soil' hypothesis revisited.* Nat Rev Cancer, 2003. **3**(6): p. 453-8.
6. Yim, E.K. and J.S. Park, *The role of HPV E6 and E7 oncoproteins in HPV-associated cervical carcinogenesis.* Cancer Res Treat, 2005. **37**(6): p. 319-24.
7. de Sanjose, S., et al., *Worldwide prevalence and genotype distribution of cervical human papillomavirus DNA in women with normal cytology: a meta-analysis.* Lancet Infect Dis, 2007. **7**(7): p. 453-9.
8. Brisson, J., et al., *Risk factors for cervical intraepithelial neoplasia: differences between low- and high-grade lesions.* Am J Epidemiol, 1994. **140**(8): p. 700-10.
9. Franceschi, S., et al., *Variations in the age-specific curves of human papillomavirus prevalence in women worldwide.* Int J Cancer, 2006. **119**(11): p. 2677-84.
10. World Health Organization., *International statistical classification of diseases and related health problems*. 10th rev., edition 2008. ed. 2009, Geneva: World Health Organization.
11. Kumar, V. and S.L. Robbins, *Robbins basic pathology*. 8th ed. 2007, Philadelphia, PA: Saunders/Elsevier. xiv, 946 p.
12. Berek, J.S. and E. Novak, *Berek & Novak's gynecology*. 15th ed. 2012, Philadelphia: Wolters Kluwer Health/Lippincott Williams & Wilkins. xix, 1539 p.
13. Woodman, C.B., S.I. Collins, and L.S. Young, *The natural history of cervical HPV infection: unresolved issues.* Nat Rev Cancer, 2007. **7**(1): p. 11-22.
14. Schorge, J.O. and J.W. Williams, *Williams gynecology*. 2008, New York: McGraw-Hill Medical. xxv, 1189 p.
15. Pecorelli, S., *Revised FIGO staging for carcinoma of the vulva, cervix, and endometrium.* Int J Gynaecol Obstet, 2009. **105**(2): p. 103-4.
16. Lai, C.H., *Management of recurrent cervical cancer.* Chang Gung Med J, 2004. **27**(10): p. 711-7.
17. Lau, Y.M., et al., *Prognostic implication of human papillomavirus types and species in cervical cancer patients undergoing primary treatment.* PLoS One, 2015. **10**(4): p. e0122557.
18. Cancer Connect. *Recurrent Cervical Cancer*. 2015 [cited 2015 29.04.2015]; Available from: http://news.cancerconnect.com/recurrent-cervical-cancer/.
19. Middleton, K., et al., *Organization of human papillomavirus productive cycle during neoplastic progression provides a basis for selection of diagnostic markers.* J Virol, 2003. **77**(19): p. 10186-201.
20. Doorbar, J., et al., *The biology and life-cycle of human papillomaviruses.* Vaccine, 2012. **30 Suppl 5**: p. F55-70.
21. Koutsky, L., *Epidemiology of genital human papillomavirus infection.* Am J Med, 1997. **102**(5A): p. 3-8.
22. Baseman, J.G. and L.A. Koutsky, *The epidemiology of human papillomavirus infections.* J Clin Virol, 2005. **32 Suppl 1**: p. S16-24.

23. Melsheimer, P., et al., *DNA aneuploidy and integration of human papillomavirus type 16 e6/e7 oncogenes in intraepithelial neoplasia and invasive squamous cell carcinoma of the cervix uteri.* Clin Cancer Res, 2004. **10**(9): p. 3059-63.
24. zur Hausen, H., *Papillomaviruses and cancer: from basic studies to clinical application.* Nat Rev Cancer, 2002. **2**(5): p. 342-50.
25. Moody, C.A. and L.A. Laimins, *Human papillomavirus oncoproteins: pathways to transformation.* Nat Rev Cancer, 2010. **10**(8): p. 550-60.
26. Schiller, J.T., P.M. Day, and R.C. Kines, *Current understanding of the mechanism of HPV infection.* Gynecol Oncol, 2010. **118**(1 Suppl): p. S12-7.
27. Doorbar, J., *Molecular biology of human papillomavirus infection and cervical cancer.* Clin Sci (Lond), 2006. **110**(5): p. 525-41.
28. Florin, L., et al., *Identification of a dynein interacting domain in the papillomavirus minor capsid protein l2.* J Virol, 2006. **80**(13): p. 6691-6.
29. Pyeon, D., et al., *Establishment of human papillomavirus infection requires cell cycle progression.* PLoS Pathog, 2009. **5**(2): p. e1000318.
30. Ziegert, C., et al., *A comprehensive analysis of HPV integration loci in anogenital lesions combining transcript and genome-based amplification techniques.* Oncogene, 2003. **22**(25): p. 3977-84.
31. Maglennon, G.A., P. McIntosh, and J. Doorbar, *Persistence of viral DNA in the epithelial basal layer suggests a model for papillomavirus latency following immune regression.* Virology, 2011. **414**(2): p. 153-63.
32. DiMaio, D. and L.M. Petti, *The E5 proteins.* Virology, 2013. **445**(1-2): p. 99-114.
33. Disbrow, G.L., J.A. Hanover, and R. Schlegel, *Endoplasmic reticulum-localized human papillomavirus type 16 E5 protein alters endosomal pH but not trans-Golgi pH.* J Virol, 2005. **79**(9): p. 5839-46.
34. Ashrafi, G.H., et al., *E5 protein of human papillomavirus type 16 selectively downregulates surface HLA class I.* Int J Cancer, 2005. **113**(2): p. 276-83.
35. Schwarz, E., et al., *Structure and transcription of human papillomavirus sequences in cervical carcinoma cells.* Nature, 1985. **314**(6006): p. 111-4.
36. Howie, H.L., R.A. Katzenellenbogen, and D.A. Galloway, *Papillomavirus E6 proteins.* Virology, 2009. **384**(2): p. 324-34.
37. Freedman, D.A. and A.J. Levine, *Nuclear export is required for degradation of endogenous p53 by MDM2 and human papillomavirus E6.* Mol Cell Biol, 1998. **18**(12): p. 7288-93.
38. Veldman, T., et al., *Human papillomavirus E6 and Myc proteins associate in vivo and bind to and cooperatively activate the telomerase reverse transcriptase promoter.* Proc Natl Acad Sci U S A, 2003. **100**(14): p. 8211-6.
39. Liu, X., et al., *The E6AP ubiquitin ligase is required for transactivation of the hTERT promoter by the human papillomavirus E6 oncoprotein.* J Biol Chem, 2005. **280**(11): p. 10807-16.
40. Jones, D.L. and K. Munger, *Interactions of the human papillomavirus E7 protein with cell cycle regulators.* Semin Cancer Biol, 1996. **7**(6): p. 327-37.
41. Dahiya, A., et al., *Role of the LXCXE binding site in Rb function.* Mol Cell Biol, 2000. **20**(18): p. 6799-805.
42. Magnaghi-Jaulin, L., et al., *Retinoblastoma protein represses transcription by recruiting a histone deacetylase.* Nature, 1998. **391**(6667): p. 601-5.
43. Brehm, A., et al., *Retinoblastoma protein recruits histone deacetylase to repress transcription.* Nature, 1998. **391**(6667): p. 597-601.
44. Shin, M.K., et al., *Human papillomavirus E7 oncoprotein overrides the tumor suppressor activity of p21Cip1 in cervical carcinogenesis.* Cancer Res, 2009. **69**(14): p. 5656-63.
45. Jones, D.L., R.M. Alani, and K. Munger, *The human papillomavirus E7 oncoprotein can uncouple cellular differentiation and proliferation in human keratinocytes by abrogating p21Cip1-mediated inhibition of cdk2.* Genes Dev, 1997. **11**(16): p. 2101-11.

46. Munger, K., et al., *The E6 and E7 genes of the human papillomavirus type 16 together are necessary and sufficient for transformation of primary human keratinocytes.* J Virol, 1989. **63**(10): p. 4417-21.
47. Jones, D.L., D.A. Thompson, and K. Munger, *Destabilization of the RB tumor suppressor protein and stabilization of p53 contribute to HPV type 16 E7-induced apoptosis.* Virology, 1997. **239**(1): p. 97-107.
48. Stoppler, H., et al., *The human papillomavirus type 16 E6 and E7 oncoproteins dissociate cellular telomerase activity from the maintenance of telomere length.* J Biol Chem, 1997. **272**(20): p. 13332-7.
49. Spardy, N., et al., *HPV-16 E7 reveals a link between DNA replication stress, fanconi anemia D2 protein, and alternative lengthening of telomere-associated promyelocytic leukemia bodies.* Cancer Res, 2008. **68**(23): p. 9954-63.
50. Duensing, A., et al., *Centrosome overduplication, chromosomal instability, and human papillomavirus oncoproteins.* Environ Mol Mutagen, 2009. **50**(8): p. 741-7.
51. Duensing, S., et al., *Human papillomavirus type 16 E7 oncoprotein-induced abnormal centrosome synthesis is an early event in the evolving malignant phenotype.* Cancer Res, 2001. **61**(6): p. 2356-60.
52. Taylor, W.R. and G.R. Stark, *Regulation of the G2/M transition by p53.* Oncogene, 2001. **20**(15): p. 1803-15.
53. Finzer, P., A. Aguilar-Lemarroy, and F. Rosl, *The role of human papillomavirus oncoproteins E6 and E7 in apoptosis.* Cancer Lett, 2002. **188**(1-2): p. 15-24.
54. Stoppler, M.C., et al., *The E5 gene of HPV-16 enhances keratinocyte immortalization by full-length DNA.* Virology, 1996. **223**(1): p. 251-4.
55. Bouvard, V., et al., *The human papillomavirus type 16 E5 gene cooperates with the E7 gene to stimulate proliferation of primary cells and increases viral gene expression.* Virology, 1994. **203**(1): p. 73-80.
56. Petti, L., L.A. Nilson, and D. DiMaio, *Activation of the platelet-derived growth factor receptor by the bovine papillomavirus E5 transforming protein.* EMBO J, 1991. **10**(4): p. 845-55.
57. Boyman, O., et al., *The pathogenic role of tissue-resident immune cells in psoriasis.* Trends Immunol, 2007. **28**(2): p. 51-7.
58. Agaiby, A.D. and M. Dyson, *Immuno-inflammatory cell dynamics during cutaneous wound healing.* J Anat, 1999. **195 (Pt 4)**: p. 531-42.
59. Kovacic, M.B., et al., *Epidemiologic analysis of histologic cervical inflammation: relationship to human papillomavirus infections.* Hum Pathol, 2008. **39**(7): p. 1088-95.
60. Hibma, M.H., *The immune response to papillomavirus during infection persistence and regression.* Open Virol J, 2012. **6**: p. 241-8.
61. Hall, J.C. and A. Rosen, *Type I interferons: crucial participants in disease amplification in autoimmunity.* Nat Rev Rheumatol, 2010. **6**(1): p. 40-9.
62. Kanodia, S., L.M. Fahey, and W.M. Kast, *Mechanisms used by human papillomaviruses to escape the host immune response.* Curr Cancer Drug Targets, 2007. **7**(1): p. 79-89.
63. Arany, I., A. Goel, and S.K. Tyring, *Interferon response depends on viral transcription in human papillomavirus-containing lesions.* Anticancer Res, 1995. **15**(6B): p. 2865-9.
64. Park, J.S., et al., *Inactivation of interferon regulatory factor-1 tumor suppressor protein by HPV E7 oncoprotein. Implication for the E7-mediated immune evasion mechanism in cervical carcinogenesis.* J Biol Chem, 2000. **275**(10): p. 6764-9.
65. Black, A.P., et al., *Human keratinocyte induction of rapid effector function in antigen-specific memory CD4+ and CD8+ T cells.* Eur J Immunol, 2007. **37**(6): p. 1485-93.

66. Stanley, M.A., *Epithelial cell responses to infection with human papillomavirus.* Clin Microbiol Rev, 2012. **25**(2): p. 215-22.
67. Ashworth, T.R., *A case of cancer in which cells similar to those in the tumours were seen in the blood after death.* The Medical Journal of Australia, 1869. **vol. 14**: p. pp. 146–147.
68. Miller, M.C., G.V. Doyle, and L.W. Terstappen, *Significance of Circulating Tumor Cells Detected by the CellSearch System in Patients with Metastatic Breast Colorectal and Prostate Cancer.* J Oncol, 2010. **2010**: p. 617421.
69. Paget, S., *The distribution of secondary growths in cancer of the breast. 1889.* Cancer Metastasis Rev, 1889. **8**(2): p. 98-101.
70. Fehm, T., et al., *Cytogenetic evidence that circulating epithelial cells in patients with carcinoma are malignant.* Clin Cancer Res, 2002. **8**(7): p. 2073-84.
71. Schroeder, A., et al., *Treating metastatic cancer with nanotechnology.* Nat Rev Cancer, 2012. **12**(1): p. 39-50.
72. Heppner, G.H., *Tumor heterogeneity.* Cancer Res, 1984. **44**(6): p. 2259-65.
73. Fidler, I.J., *Metastasis: guantitative analysis of distribution and fate of tumor embolilabeled with 125 I-5-iodo-2'-deoxyuridine.* J Natl Cancer Inst, 1970. **45**(4): p. 773-82.
74. Gay, L.J. and B. Felding-Habermann, *Contribution of platelets to tumour metastasis.* Nat Rev Cancer, 2011. **11**(2): p. 123-34.
75. Ksiazkiewicz, M., A. Markiewicz, and A.J. Zaczek, *Epithelial-mesenchymal transition: a hallmark in metastasis formation linking circulating tumor cells and cancer stem cells.* Pathobiology, 2012. **79**(4): p. 195-208.
76. Weis, S., et al., *Endothelial barrier disruption by VEGF-mediated Src activity potentiates tumor cell extravasation and metastasis.* J Cell Biol, 2004. **167**(2): p. 223-9.
77. Gupta, G.P., et al., *Mediators of vascular remodelling co-opted for sequential steps in lung metastasis.* Nature, 2007. **446**(7137): p. 765-70.
78. Joyce, J.A. and J.W. Pollard, *Microenvironmental regulation of metastasis.* Nat Rev Cancer, 2009. **9**(4): p. 239-52.
79. Cristofanilli, M., et al., *Circulating tumor cells, disease progression, and survival in metastatic breast cancer.* N Engl J Med, 2004. **351**(8): p. 781-91.
80. de Bono, J.S., et al., *Circulating tumor cells predict survival benefit from treatment in metastatic castration-resistant prostate cancer.* Clin Cancer Res, 2008. **14**(19): p. 6302-9.
81. Hayes, D.F. and J. Smerage, *Is there a role for circulating tumor cells in the management of breast cancer?* Clin Cancer Res, 2008. **14**(12): p. 3646-50.
82. Kasimir-Bauer, S., *Circulating tumor cells as markers for cancer risk assessment and treatment monitoring.* Mol Diagn Ther, 2009. **13**(4): p. 209-15.
83. Pantel, K. and R.H. Brakenhoff, *Dissecting the metastatic cascade.* Nat Rev Cancer, 2004. **4**(6): p. 448-56.
84. Wittekind, C. and M. Neid, *Cancer invasion and metastasis.* Oncology, 2005. **69 Suppl 1**: p. 14-6.
85. Pantel, K., C. Alix-Panabieres, and S. Riethdorf, *Cancer micrometastases.* Nat Rev Clin Oncol, 2009. **6**(6): p. 339-51.
86. Obermayr, E., et al., *Assessment of a six gene panel for the molecular detection of circulating tumor cells in the blood of female cancer patients.* BMC Cancer, 2010. **10**: p. 666.
87. Fagundes, H., et al., *Distant metastases after irradiation alone in carcinoma of the uterine cervix.* Int J Radiat Oncol Biol Phys, 1992. **24**(2): p. 197-204.
88. Pfitzner, C., et al., *Digital-Direct-RT-PCR: a sensitive and specific method for quantification of CTC in patients with cervical carcinoma.* Sci Rep, 2014. **4**: p. 3970.
89. Hong, B. and Y. Zu, *Detecting circulating tumor cells: current challenges and new trends.* Theranostics, 2013. **3**(6): p. 377-94.

90. Lianidou, E.S. and A. Markou, *Circulating tumor cells in breast cancer: detection systems, molecular characterization, and future challenges.* Clin Chem, 2011. **57**(9): p. 1242-55.
91. UniProt. *Epithelial cell adhesion molecule*. 1990 07.01.2015 [cited 2015 20.03.]; Available from: http://www.uniprot.org/uniprot/P16422.
92. Rao, C.G., et al., *Expression of epithelial cell adhesion molecule in carcinoma cells present in blood and primary and metastatic tumors.* Int J Oncol, 2005. **27**(1): p. 49-57.
93. van der Gun, B.T., et al., *EpCAM in carcinogenesis: the good, the bad or the ugly.* Carcinogenesis, 2010. **31**(11): p. 1913-21.
94. Hu, M., et al., *Functional polymorphism in the EpCAM gene is associated with occurrence and advanced disease status of cervical cancer in Chinese population.* Mol Biol Rep, 2012. **39**(7): p. 7303-9.
95. Munz, M., et al., *The carcinoma-associated antigen EpCAM upregulates c-myc and induces cell proliferation.* Oncogene, 2004. **23**(34): p. 5748-58.
96. Hanukoglu, I. and E. Fuchs, *The cDNA sequence of a Type II cytoskeletal keratin reveals constant and variable structural domains among keratins.* Cell, 1983. **33**(3): p. 915-24.
97. Ditzel, H.J., et al., *Cancer-associated cleavage of cytokeratin 8/18 heterotypic complexes exposes a neoepitope in human adenocarcinomas.* J Biol Chem, 2002. **277**(24): p. 21712-22.
98. Stewart, C.J., et al., *Cytokeratin 19 expression in normal endometrium and in low-grade endometrioid adenocarcinoma of the endometrium.* Int J Gynecol Pathol, 2011. **30**(5): p. 484-91.
99. Yuan, C.C., et al., *Elevated cytokeratin-19 expression associated with apoptotic resistance and malignant progression of human cervical carcinoma.* Apoptosis, 1998. **3**(3): p. 161-9.
100. UniProt. *CCNE2 protein*. 2012 04.03.2015 [cited 2015 20.03.]; Available from: http://www.uniprot.org/uniprot/I6L961.
101. Donnellan, R. and R. Chetty, *Cyclin E in human cancers.* FASEB J, 1999. **13**(8): p. 773-80.
102. Zerfass, K., et al., *Sequential activation of cyclin E and cyclin A gene expression by human papillomavirus type 16 E7 through sequences necessary for transformation.* J Virol, 1995. **69**(10): p. 6389-99.
103. Ohtani, K., J. DeGregori, and J.R. Nevins, *Regulation of the cyclin E gene by transcription factor E2F1.* Proc Natl Acad Sci U S A, 1995. **92**(26): p. 12146-50.
104. McIntyre, M.C., M.N. Ruesch, and L.A. Laimins, *Human papillomavirus E7 oncoproteins bind a single form of cyclin E in a complex with cdk2 and p107.* Virology, 1996. **215**(1): p. 73-82.
105. Tae Kim, Y., et al., *Expression of cyclin E and p27(KIP1) in cervical carcinoma.* Cancer Lett, 2000. **153**(1-2): p. 41-50.
106. UniProt. *Cyclin-dependent kinase inhibitor 2A*. 1995 04.03.2015 [cited 2015 20.03.]; Available from: http://www.uniprot.org/uniprot/P42771.
107. Hwang, S.J. and K.R. Shroyer, *Biomarkers of cervical dysplasia and carcinoma.* J Oncol, 2012. **2012**: p. 507286.
108. Klaes, R., et al., *Overexpression of p16(INK4A) as a specific marker for dysplastic and neoplastic epithelial cells of the cervix uteri.* Int J Cancer, 2001. **92**(2): p. 276-84.
109. Keating, J.T., et al., *Ki-67, cyclin E, and p16INK4 are complimentary surrogate biomarkers for human papilloma virus-related cervical neoplasia.* Am J Surg Pathol, 2001. **25**(7): p. 884-91.
110. UniProt. *UniProt - Receptor-type tyrosine-protein phosphatase C*. 1988 January 7, 2015 [cited 2015 20.03.2015]; Available from: http://www.uniprot.org/uniprot/P08575.

111. Hristozova, T., et al., *A simple multicolor flow cytometry protocol for detection and molecular characterization of circulating tumor cells in epithelial cancers.* Cytometry A, 2012. **81**(6): p. 489-95.
112. Brandt, B. and C. Griwatz, *Two-layer buoyant density centrifugation gradient for enrichment of prostate-derived cells and cell clusters from peripheral blood.* Clin Chem, 1996. **42**(11): p. 1881-2.
113. Carpenter, A.E., et al., *CellProfiler: image analysis software for identifying and quantifying cell phenotypes.* Genome Biol, 2006. **7**(10): p. R100.
114. Gupta, G.P. and J. Massague, *Cancer metastasis: building a framework.* Cell, 2006. **127**(4): p. 679-95.
115. Delgado, G., et al., *Prospective surgical-pathological study of disease-free interval in patients with stage IB squamous cell carcinoma of the cervix: a Gynecologic Oncology Group study.* Gynecol Oncol, 1990. **38**(3): p. 352-7.
116. Zaino, R.J., et al., *Histopathologic predictors of the behavior of surgically treated stage IB squamous cell carcinoma of the cervix. A Gynecologic Oncology Group study.* Cancer, 1992. **69**(7): p. 1750-8.
117. Burghardt, E., et al., *Results of surgical treatment of 1028 cervical cancers studied with volumetry.* Cancer, 1992. **70**(3): p. 648-55.
118. Stehman, F.B., et al., *Carcinoma of the cervix treated with radiation therapy. I. A multi-variate analysis of prognostic variables in the Gynecologic Oncology Group.* Cancer, 1991. **67**(11): p. 2776-85.
119. Scher, H.I., et al., *Circulating tumour cells as prognostic markers in progressive, castration-resistant prostate cancer: a reanalysis of IMMC38 trial data.* Lancet Oncol, 2009. **10**(3): p. 233-9.
120. Pierga, J.Y., et al., *High independent prognostic and predictive value of circulating tumor cells compared with serum tumor markers in a large prospective trial in first-line chemotherapy for metastatic breast cancer patients.* Ann Oncol, 2012. **23**(3): p. 618-24.
121. Ma, X.L., et al., *Meta-analysis of circulating tumor cells as a prognostic marker in lung cancer.* Asian Pac J Cancer Prev, 2012. **13**(4): p. 1137-44.

8 Table of figures

9 List of tables

10 Abstract

Cervical cancer is the fourth most common cancer in women worldwide. Almost all cervical cancer cases (99.7%) are induced by a Human papillomavirus (HPV) infection, whereby the genotypes HPV16 and HPV18 are of most clinical abundance. In advanced stages, tumor derived cells may invade into the vascular system. This circulating tumor cells (CTCs) are capable of settling in secondary organs and establishing micrometastases. Often micrometastases survive clinical treatment, leading to clinical relapse and further off scaling CTCs. In terms of clinical recurrence, micrometastases are difficult to determine by imaging methods. Therefore, the detection of CTCs might facilitate an additional diagnostic process, capable to indicate relapse at an earlier time point. The aim of this project was the development of a cervical cancer antigen-specific CTC panel, which could be applied in a five-color immunofluorescence staining for detection of CTCs in a density gradient enriched blood fraction. This would represent an alternative for monitoring of cervical cancer patients. In addition, a computational image analysis, capable of marker-specific CTC identification should be elaborated. To accomplish this, six CTC and one immune cell specific markers were tested. As result two five-color immunofluorescence panels were successfully established, allowing the simultaneous detection and characterization of cervical cancer derived CTCs via the markers: Cytokeratin, EpCAM, HPV16 E7 (panel 1) or Cytokeratin, Cyclin E2, p16 (panel 2). In addition either panel implies CD45 as panleukocyte marker. Both panels were utilized on previously processed blood samples of 59 cervical cancer patients, which were obtained at time point of primary diagnosis. The analysis resulted in 10/59 (16.9%) of samples, where CTCs could be identified with either one of the applied markers. Panel-wise, 5/59 (8.5%) samples were positive for panel 1 and 6/59 (10.2%) for panel 2 markers. In 1/59 (1.7%) sample CTC detection based on both panels was achieved. Thereby, the specificity and reliability differed among the individual markers. Cytokeratin and EpCAM exhibited the highest reliability and specificity, HPV16 E7 is suitable, but did not add further information and both HPV-surrogate markers, p16 and Cyclin E2, are not appropriate for a specific CTC detection. For the automated image evaluation, a CellProfiler pipeline was developed. The application on patients' samples resulted in an exponential overestimation of CTCs. However, the threshold adaption to actual CTC fluorescence values attenuated the overestimation and significantly reduced the false positive count. Generation of a cervical cancer specific marker panel for five-color immunofluorescence and the general feasibility of an automated image evaluation could be shown in this study. Thus, the basis of a possible relapse monitoring could be achieved.

Further evaluation of the clinical significance of the obtained results will be of high interest, to assess a possible prognostic influence of the presence of CTCs at time of primary diagnosis and to see whether earlier relapse diagnosis is possible. In the course of this thesis, relapse information could only be received in a limited number of patients due to the time frame, which does not allow a statistical analysis.

11 Zusammenfassung

Das Zervixkarzinom ist die vierthäufigste Tumorentität weltweit unter weiblichen Krebspatientinnen. Nahezu alle Zervixkarzinome (99.7%) sind auf eine Infektion der Cervix uteri mit humanen Papillomviren (HPV) zurückzuführen. Größte klinische Bedeutung haben dabei die HPV-Genotypen HPV16 und HPV18. Mit fortschreitendem Verlauf einer Krebserkrankung können sich einzelnen Tumorzellen abschilfern und ins Blutgefäßsystem gelangen. Diese zirkulierenden Tumorzellen (CTC) können sich in sekundären Organen absetzen und schwer zu therapierende Mikrometastasen ausbilden. Im Fall von klinischer Rezidivierung ist eine Erkennung dieser Mikrometastasen mittels bildgebender Verfahren schwierig. Eine Detektion von CTCs könnte daher eine zusätzliche Methode zur Rezidivüberwachung darstellen, die eine Indikation bereits zu einem früheren Zeitpunkt ermöglicht. Das Ziel der vorliegenden Arbeit war daher die Entwicklung eines antigen-spezifischen Clusters zur Identifizierung von CTCs in einer angereicherten Fraktion des Blutes von Zervixkarzinom-Patientinnen, mittels einer parallelen fünffachen Immunfluoreszenzfärbung. Zusätzlicher Inhalt dieser Arbeit war die Entwicklung einer computerbasierten Bildauswertung zur CTC Identifikation. Für den Cluster wurden sechs zervixkarzinom- und ein immunzellspezifischer Marker evaluiert. Daraus konnten zwei fünffache Immunfluoreszenzfärbungen erstellt werden, die entweder Cytokeratin, EpCAM und HPV16 E17 (Cluster 1) oder p16, Cyclin E2 und Cytokeratin (Cluster 2) als Zervixkarzinommarker und CD45 als Immunmarker detektieren und charakterisieren können. Die zum Zeitpunkt der Primärdiagnose entnommenen Patientenproben (n=59) wurden unter Anwendung beider Cluster gefärbt. In 10 (16,9%) Patientinnen konnten CTCs nachgewiesen werden, wobei in 5 (8,5%) Proben CTCs mittels Cluster 1 und in 6 (10,2%) Proben mittels Cluster 2 identifiziert wurden. Dabei zeigte sich, dass die Marker Cytokeratin und EpCAM die höchste Spezifität und Reliabilität aufweisen, HPV16 E7 hingegen fügt keine zusätzlichen Informationen hinzu und beide HPV-surrogat Marker, p16 und Cyclin E2, sind nur eingeschränkt für die CTC Detektion geeignet. Für die automatisierte Bildauswertung wurde eine Pipeline in der Software „CellProfiler“ erstellt. Bei der Auswertung von Patientenproben resultierte diese in einer exponentiellen Überschätzung der CTC-Anzahl. Durch eine Anpassung der Fluoreszenz-Grenzwerte an exakte CTC-Werte konnte die Überschätzung deutlich reduziert werden und gleichzeitig auch eine signifikante Reduktion der Falsch-Positiv-Rate erreicht werden. Die Etablierung eines antigen-spezifischen Clusters zur Identifizierung von Zervixkarzinom-CTCs und die Realisierbarkeit einer automatisierten CTC-Detektion konnten in dieser Arbeit erreicht werden. Damit konnte eine Basis für eine mögliche Methode zu Rezidiv-Überwachung geschaffen werden.

Eine ausführliche Korrelation der erhaltenen Ergebnisse mit klinischen Daten könnte die Prognose erlauben, ob CTCs zum Zeitpunkt der primären Diagnose einen Einfluss auf den weiterführenden Krankheitsverlauf haben und ob die Rezidivierung früher nachweisbar ist. Aufgrund des Zeitrahmens dieser Arbeit waren Rezidiv-Daten lediglich in einigen Fällen vorhanden, was eine solche statistische Analyse nicht zuließ.

12 Acknowledgements

I want to thank Robert Zeillinger for giving me the opportunity to work on this masters' thesis and providing me magnificent scientific support. A very special tank goes to my supervisor Elisabeth Maritschnegg, who conducted and promoted me throughout the whole project. Elisabeth's advice and scientific support in many discussions were extremely instructive and valuable. I also want to thank the whole group of the Molecular Oncology for the collaboration, helpfulness and the great atmosphere to work in.

Further, I would appreciate Marion Gröger and Sabine Rauscher of the Imaging Core Facility for providing the TissueFAXS/LSM 780, technical support and their general cooperativeness.

My deepest gratitude is dedicate to my whole family, especially my parents, and Sophie, who supported my unconditionally and were solidly behind me.

13 Curriculum Vitae

Personal Data

Date and place of birth	24.05.1987 Wolfsburg, Germany
Nationality	German

Education

06/2015	Medical University of Vienna Masters' thesis: *Detection of Cervical Cancer Derived Circulating Tumor Cells in the Peripheral Blood*
10/2013 – 06/2015	Master studies in Molecular microbiology, microbial ecology and immunobiology University of Vienna
06/2013	Max F. Perutz Laboratories Bachelors' thesis: *The effect of Mss116p on the splicing efficiency of the mitochondrial yeast bI5 intron and the subsequent S. cerevisiae growth ability*
03/2010 – 06/2013	Bachelor studies in Microbiology and Genetics University of Vienna
08/2007 – 01/2010	Apprenticeship as information technology officer Norddeutsche Landesbank Girozentrale
06/2006	High-school diploma Theodor-Heuss-Gymnasium Wolfsburg

Working Experience

06/2014 – 05/2015	Medical University of Vienna Master thesis at the department of Gynecology and Obstetrics Molecular Oncology
02/2014 – 06/2014	Medical University of Vienna Traineeship at the department of Gynecology and Obstetrics Molecular Oncology
04/2012 – 06/2012	University of Vienna Bachelor thesis at Max F. Perutz Laboratories Institute for Biochemistry and Biophysics

Accolades

2014 – 2015	Master's Degree Scholarships Medical University of Vienna
2013 – 2014	Performance Scholarship University of Vienna

14 Supplementary data

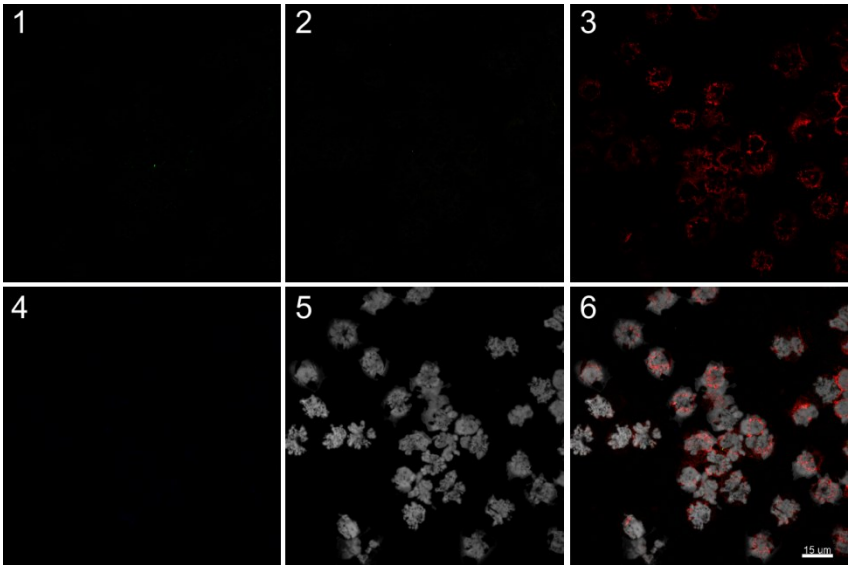

Figure 25: IF staining of negative control (panel 1).(1) EpCAM – green, (2) HPV16 E7 – yellow, (3) CD45 – red, (4) pan Cytokeratin – blue, (5) DAPI – grey, (6) merge.

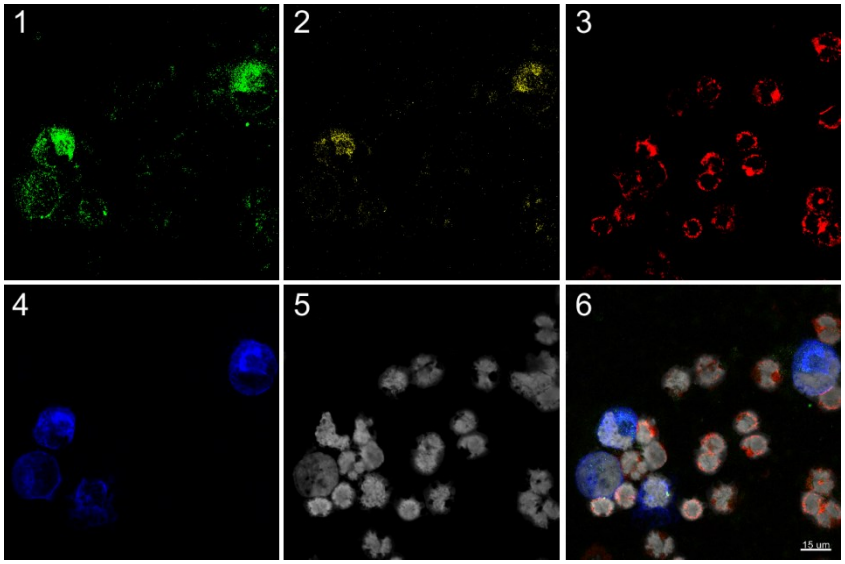

Figure 26: IF staining of positive control (panel 1).(1) EpCAM – green, (2) HPV16 E7 – yellow, (3) CD45 – red, (4) pan Cytokeratin – blue, (5) DAPI – grey, (6) merge.

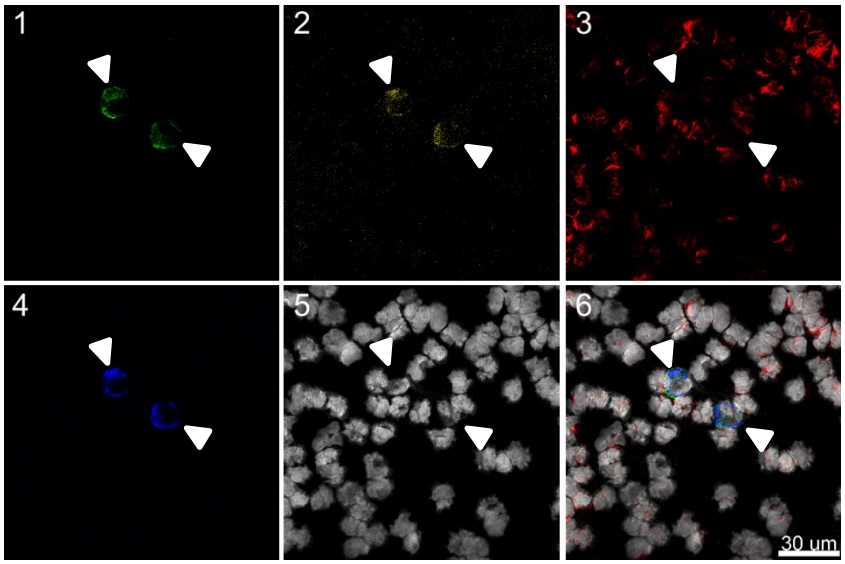

Figure 27: IF staining of patients‘ CTC (13625_1).(1) EpCAM – green, (2) HPV16 E7 – yellow, (3) CD45 – red, (4) pan Cytokeratin – blue, (5) DAPI – grey, (6) merge. Arrows indicating cervical cancer derived CTCs.

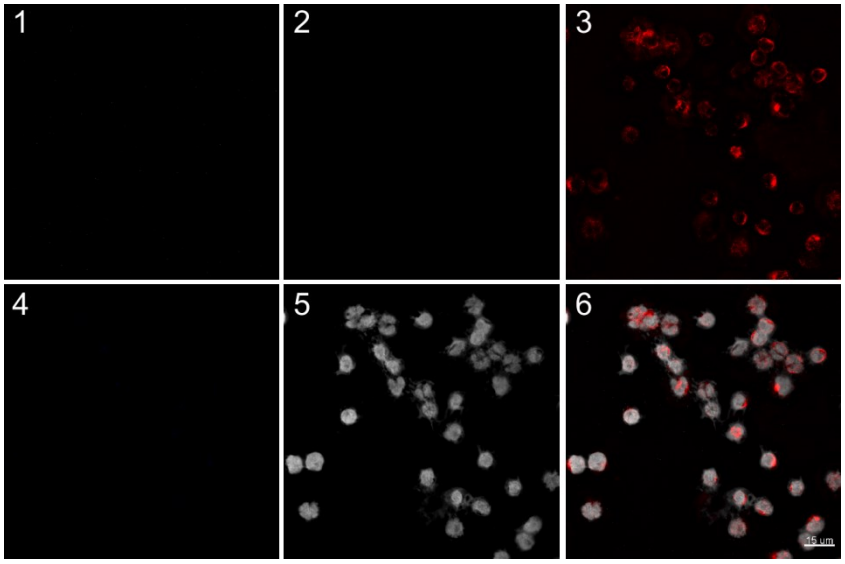

Figure 28: IF staining of negative control (panel 2).(1) Cyclin E2 – green, (2) p16 – yellow, (3) CD45 – red, (4) pan Cytokeratin – blue, (5) DAPI – grey, (6) merge.

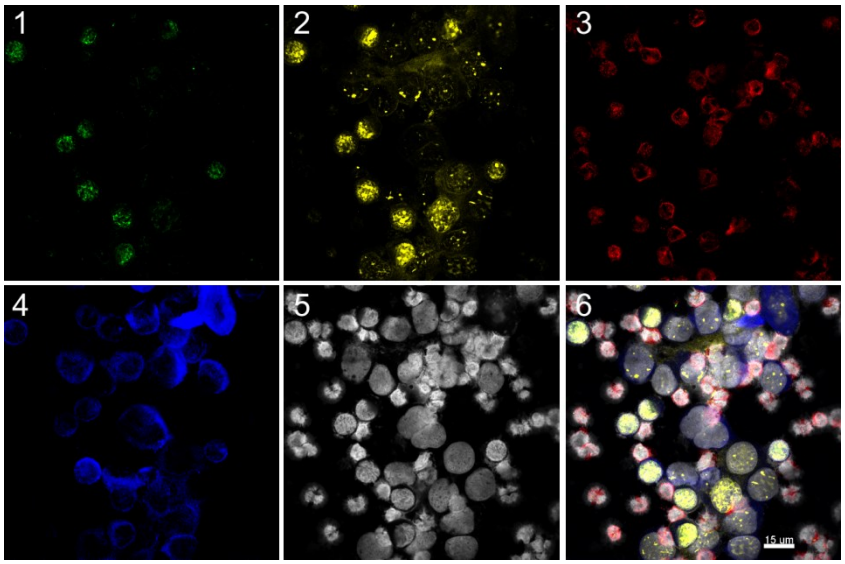

Figure 29: IF staining of positive control (panel 2).(1) Cyclin E2 – green, (2) p16 – yellow, (3) CD45 – red, (4) pan Cytokeratin – blue, (5) DAPI – grey, (6) merge.

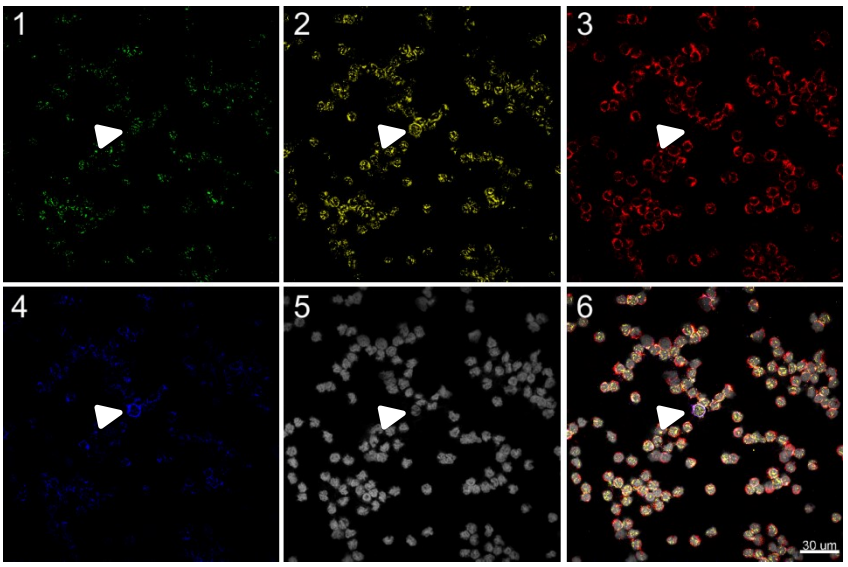

Figure 30: IF staining of patients‘ CTC (13625). (1) p16 – green, (2) Cyclin E2 – yellow, (3) CD45 – red, (4) pan Cytokeratin – blue, (5) DAPI – grey, (6) merge. Arrow indicates cervical cancer derived CTCs.

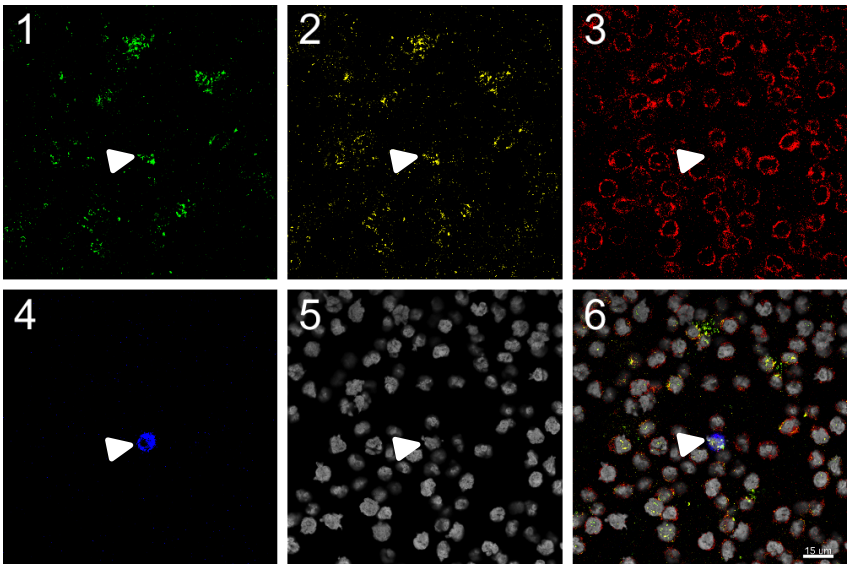

Figure 31: IF staining of patients' CTC (14528).(1) p16 – green, (2) Cyclin E2 – yellow, (3) CD45 – red, (4) pan Cytokeratin – blue, (5) DAPI – grey, (6) merge. Arrow indicates cervical cancer derived CTCs.

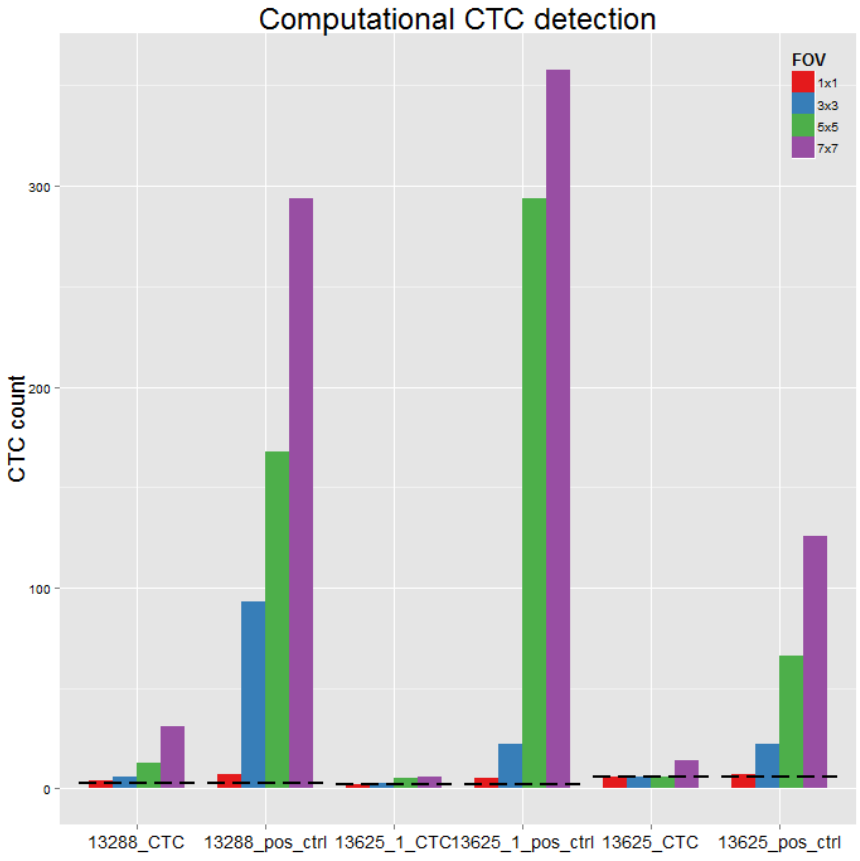

Figure 32: CellProfiler provided CTC detection. CellProfiler field-of-view-wise CTC count with CTC and positive-control-adapted thresholds. Horizontal dashed line indicates the true positive CTC rate in the sample.